Eur. Phys. J. D **22**, 81–97 (2003)
DOI: 10.1140/epjd/e2002-00224-x

THE EUROPEAN PHYSICAL JOURNAL D

Cooling efficiency in collisions between Pd_{13} and He, Ne, Ar and Kr

J. Westergren[1,a], S. Nordholm[2], and A. Rosén[1]

[1] School of Physics and Engineering Physics, Department of Experimental Physics, Chalmers University of Technology and Göteborg University, 412 96 Göteborg, Sweden
[2] Department of Chemistry, Göteborg University, 412 96 Göteborg, Sweden

Received 28 September 2001 / Received in final form 8 August 2002
Published online 12 November 2002 –

Abstract. The cooling of the metal cluster Pd_{13} in an atmosphere of rare gas has been studied by means of computer simulation. By simulation, the average energy transfer in collisions between one cluster and one gas atom has been obtained. Emphasis has been placed on conditions when the temperatures of the colliding species are almost equal. All modes of motion, inclusive the translation, must be considered in order to obtain vanishing energy transfer at equilibrium. A simulation scheme is presented by which the energy transfer is zero to the cluster when the gas and the cluster temperatures are equal. At equilibrium the energy transfer does however not vanish for all impact parameters. In the collisions with Pd_{13}, the cluster is heated by collisions with a small impact parameter but equally cooled by collisions with a large impact parameter. Argon and krypton are found to cool Pd_{13} equally efficiently while neon and helium are less efficient cooling agents.

PACS. 34.10.+x General theories and models of atomic and molecular collisions and interactions (including statistical theories, transition state, stochastic and trajectory models, etc.) – 34.30.+h Intramolecular energy transfer; intramolecular dynamics; dynamics of van der Waals molecules – 36.40.-c Atomic and molecular clusters

1 Introduction

In cluster experiments it has been observed that many properties of free clusters, *i.e.* unsupported clusters in near-vacuum, depend on the internal cluster temperature. For instance, the ionization potential [1–3], reactivity [4] and magnetic moments [5] show dependence on the temperature. Therefore, there is an experimental need to know the temperature of a cluster in a cluster beam. Methods have been developed to vary the temperature of clusters by use of a surrounding gas serving as a heat bath [6,7]. Schmidt *et al.* [7] have used a heat bath to thermalize sodium clusters at various temperatures. From experiments, they have then been able to determine the heat capacity of sodium clusters as a function of temperature. Using the fact that the transition from rigid to molten cluster leads to a maximum in the heat capacity, they have also obtained the melting temperature for various cluster sizes. It is generally assumed that when a cluster is cooled in a heat bath, it is brought into thermal equilibrium with the gas. In previous papers [8–10], the number of collisions required to cool the metal clusters Pd_{13} and Pd_{55} in a helium atmosphere was investigated by means of molecular dynamics simulation. In this work the simulations are refined and extended to include also collisions between Pd_{13} and the rare gases Ne, Ar and Kr.

In order to computationally resolve the cooling process of a cluster in a gas atmosphere the average energy transfer and the cluster heat capacity must be known at different cluster temperatures. In this work, molecular dynamics simulation has been used to calculate the average energy transfer. The heat capacity of Pd_{13} has been calculated in previous work of ours [11] using Monte Carlo simulations.

The emphasis of this work is on the study of collisions using different rare gas atoms. Collisions involving atoms and molecules have been a field of importance in chemistry and physics throughout the twentieth century and it still attracts much attention. One of the reasons is that in the RRKM theory [12] of unimolecular reactions, the energy transfer in the collisions is one of the two mechanisms determining the reaction rate. In such investigations the aim is to determine the kernel function $P(E', E)$ which is the probability of changing the energy from E to E' in a collision [13]. However, collisions are studied for many other reasons. For instance, deposition of clusters on substrates is a topic which employs many scientists these days [14–16]. Collisions between clusters and rare gas atoms are in a sense an intermediate case

[a] e-mail: JanW@phc.gu.se

between molecule–molecule and molecule–surface collisions. The cluster is sufficiently large so that only a fraction of the cluster participates in the encounter. On the other hand, the cluster is sufficiently small, that the collisions will significantly affect the cluster, for instance to cool it.

In our previous publications [8–10] on collisions the translational and rotational energy of the cluster was initially zero. Hence, these degrees of freedom were always heated and therefore, the energy transfer was not precisely zero when the initial gas and cluster temperatures were equal. In the study of cooling, energy transfer data near equilibrium is required. Hence, the non-zero energy transfer at equilibrium in our earlier publications is a problem. In the present work a new simulation scheme to generate correct initial configurations and momenta of cluster and gas atom is derived. Indeed, the equilibrium condition of zero energy transfer at equal temperatures is now satisfied.

This paper is organized as follows. In Section 2 the differential equation that governs the temperature decay is formulated. A detailed derivation of the distributions required for the simulations are presented in Appendix. The results of the heat capacity calculations for Pd_{13} are presented in Section 3. The simulation of the energy transfer is described in Section 4. In Section 5 calculations of collision cross-section and collision frequency is presented. In Section 6 the results are given and conclusion are found in Section 7.

2 The cooling equation

The process we want to simulate is the cooling of a dilute component of clusters in a low-pressure atmosphere of rare gas. The lowest gas temperature in our calculations is 100 K. This is below the critical temperature of argon and krypton. But the pressure we consider (100 mbar) is below the vapor pressure at 100 K (3 300 mbar for Ar and 130 mbar for Kr [17]). Thus the rare gases are always in the gas phase.

With the condition that the cluster concentration is much lower than the gas concentration, the clusters will mostly collide with rare gas atoms, and very rarely with other clusters. Furthermore, since the rare gas pressure is low, the clusters will seldom collide with two gas atoms simultaneously. The rare gas atoms may be trapped by the attractive potential when the gas and cluster are cold. In such cases the gas atom makes multiple encounters with the cluster before it eventually leaves. In the most extreme case of cold krypton and cold Pd_{13} only 1.5% of the collisions lasted longer than the average time between collisions (at 100 mbar). Hence, collisions between Pd_{13} and two gas atoms simultaneously are very rare.

The rare gas has a fixed temperature T_g and the clusters are initially at temperature $T_c(0)$. We assume that the translational and the internal (internal = vibrational + rotational) modes of motion are in thermal equilibrium at time $t = 0$. Assuming that all degrees of freedom of the cluster are in equilibrium after each collision, the cooling of the clusters can be described by the following differential equation:

$$\mathrm{d}\langle E\rangle = c_v(T_c)\,\mathrm{d}T_c = \langle \Delta E\rangle_{T_c,T_g}\cdot z(T_c,T_g,P_g)\,\mathrm{d}t. \quad (1)$$

Here $c_v(T_c)$ is the heat capacity of the cluster at the cluster temperature T_c. $\langle \Delta E\rangle_{T_c,T_g}$ is the average energy transfer to the cluster per collision and $z(T_c,T_g,P_g)$ is the average number of collisions experienced by one cluster per unit time when the cluster and gas temperatures are T_c and T_g, respectively, and the gas pressure is P_g.

Note, however, that the energy transfer is expected to be more efficient to the translation than to the internal modes of motion. Also in our simulations we have observed that

$$\left|\frac{\langle \Delta E_{trans}\rangle}{c_{trans}}\right| > \left|\frac{\langle \Delta E_{int}\rangle}{c_{int}}\right| \Rightarrow \left|\frac{\mathrm{d}T_{trans}}{\mathrm{d}t}\right| > \left|\frac{\mathrm{d}T_{int}}{\mathrm{d}t}\right|. \quad (2)$$

Here $c_{trans} = 3k_B/2$ and $c_{int} = c_v - c_{trans}$ are the heat capacities of the translational and internal modes, respectively. T_{trans} is the translational temperature and is given by

$$3k_B T_{trans}/2 = \langle E_{trans}\rangle, \quad (3)$$

and T_{int} is the internal temperature given by

$$\int_0^{T_{int}} c_{int}(x)\,\mathrm{d}x = \langle E_{int}\rangle_{T_{int}} - E_0, \quad (4)$$

where $E_0 = -34.6$ eV is the minimum potential energy of Pd_{13} and k_B is Boltzmann's constant. Shortly after the cooling has started T_{trans} will be lower than T_{int}. Therefore the cooling process ought to be studied with T_{trans} and T_{int} being free to differ. The cooling equation as in equation (1) must then be replaced by a system of coupled differential equations

$$\begin{cases} \mathrm{d}\langle E\rangle_{trans} = c_{trans}(T_{trans})\,\mathrm{d}T_{trans} \\ \qquad\qquad = \langle \Delta E_{trans}\rangle_{T_g,T_{trans},T_{int}}\cdot z(T_{trans},T_g)\,\mathrm{d}t \\ \mathrm{d}\langle E\rangle_{int} = c_{int}(T_{int})\,\mathrm{d}T_{int} \\ \qquad\qquad = \langle \Delta E_{int}\rangle_{T_g,T_{trans},T_{int}}\cdot z(T_{trans},T_g)\,\mathrm{d}t \end{cases}. \quad (5)$$

Here $\langle \Delta E_{trans}\rangle_{T_g,T_{trans},T_{int}}$ and $\langle \Delta E_{int}\rangle_{T_g,T_{trans},T_{int}}$ are the average energy transfer to the translational and to the internal degrees of freedom of the cluster, respectively, at the temperatures T_g, T_{trans} and T_{int}.

In this paper we will assume that the rotational and vibrational temperatures are in equilibrium at all times. The rotational motion is in the cluster decoupled from the vibrational motion by the conservation of angular momentum. However, the anharmonic vibrational-rotational coupling causes the rotational and vibrational energies to vary in an oscillatory manner. Despite our present assumption we believe that vibrational and rotational energies generally differ in experiments. As a matter of fact, it has

been observed that the vibrations are warmer after the cluster aggregation [18,19] in the laser vaporization technique [20,21]. Hence the rotational and vibrational temperatures are not even equal as the clusters enter the heat bath. However, the rotational degrees of freedom are few in comparison with the vibrational ones and a separation of rotational and vibrational temperatures would make the calculation even more complex. Therefore we assume equilibrium in the internal degrees of freedom. In contrast, the separation of translational and internal degrees of freedom in the calculations is simple.

In this paper the temperature decay from $T_{\rm trans} = T_{\rm int} = 1\,300$ K in a rare gas atmosphere of 100 K and 300 K, respectively, will be followed by computation. In order to calculate how the cluster temperatures decrease with time, the following functions must be known: $c_{\rm trans}$ and $c_{\rm int}$ in the temperature interval 100 K to 1 300 K, $z\left(T_{\rm trans}, T_{\rm g}\right)$ when $T_{\rm trans} \in [100\text{ K}, 1\,300\text{ K}]$ and $T_{\rm g} = 100$ K and 300 K, respectively. Moreover, $\langle \Delta E_{\rm trans} \rangle_{T_{\rm g}, T_{\rm trans}, T_{\rm int}}$ and $\langle \Delta E_{\rm int} \rangle_{T_{\rm g}, T_{\rm trans}, T_{\rm int}}$ must be known for a grid of temperatures covering the intervals $100\text{ K} \leq T_{\rm trans} \leq T_{\rm int} \leq 1\,300$ K and $T_{\rm g} = 100$ and 300 K, respectively. When $T_{\rm trans} = T_{\rm int}$ we will write $T_{\rm c}$ for both in the text.

3 The heat capacity

For a system in canonical equilibrium, in which the volume, temperature and number of particles are fixed, the heat capacity at constant volume is proportional to the fluctuations in energy

$$c_{\rm v}\left(T_{\rm c}\right) = \frac{{\rm Var}\left[E\right]}{k_{\rm B}T_{\rm c}^2} = \frac{\left\langle E^2 \right\rangle_{T_{\rm c}} - \left\langle E \right\rangle_{T_{\rm c}}^2}{k_{\rm B}T_{\rm c}^2}\,. \tag{6}$$

The contribution to the heat capacity from the kinetic energy is $c_{\rm v,kin} = 3nk_{\rm B}/2$, where $n = 13$ is the number of atoms in the cluster. The contribution from the potential energy has been obtained in Monte Carlo simulations [11]. In these simulations a large number of spatial configurations, $\{\mathbf{R}\}$, were generated according to the Boltzmann probability distribution

$$f\left(\mathbf{R}\right) \propto \exp\left(-\frac{U\left(\mathbf{R}\right)}{k_{\rm B}T_{\rm c}}\right), \tag{7}$$

where $U\left(\mathbf{R}\right)$ is the potential energy of configuration $\mathbf{R}$. A configuration is a vector of all spatial coordinates of the cluster atoms, $\mathbf{R} = [x_1, y_1, z_1, x_2, ..., z_n]$. The variance in potential energy is obtained from the Monte Carlo simulations as

$${\rm Var}\left[U\right] = \left\langle U^2 \right\rangle - \left\langle U \right\rangle^2, \tag{8}$$

where the averages are over all the spatial configurations $\{\mathbf{R}\}$. In the canonical ensemble the kinetic and potential energies are independent, thus we finally obtain the total heat capacity as

$$c_{\rm v}\left(T_{\rm c}\right) = \frac{3nk_{\rm B}}{2} + \frac{\left\langle U^2 \right\rangle - \left\langle U \right\rangle^2}{k_{\rm B}T_{\rm c}^2}\,. \tag{9}$$

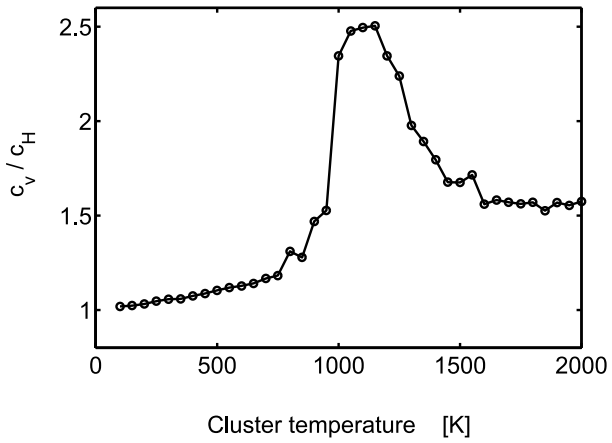

Fig. 1. The heat capacity at constant volume is shown for Pd_{13} divided by the harmonic heat capacity, $c_{\rm H} = 36k_{\rm B}$. The results are from Monte Carlo simulations [11].

The heat capacity obtained from the Monte Carlo simulations is shown in Figure 1. At very low temperature the heat capacity approaches the harmonic limit, $c_{\rm H} = 36k_{\rm B}$, when the vibrations are all harmonic. When the cluster temperature is increased, the vibrations become more and more anharmonic (leading to a higher heat capacity) until the cluster finally starts to melt. A finite system does not melt at a single temperature by a proper phase transition [22–24], but rather melts over a temperature interval which in the case of Pd_{13} extends approximately from 900 to 1 300 K. A more detailed description of the heat capacity calculations from Monte Carlo simulations can be found in a previous publication of ours [11].

4 Energy transfer in collisions between Pd_{13} and rare gases

4.1 Initial positions and velocities

The average energy transfer to the translational and the internal degrees of freedom, respectively, must be calculated in order to solve the cooling equation (Eq. (5)). We do this by means of molecular dynamics simulation of a large number of collisions between a single gas atom and a single cluster. The trajectories are integrated using the Runge-Kutta fourth order algorithm [25] with the timesteps 0.5, 0.5, 0.75 and 1.0 fs for the collisions with He, Ne, Ar and Kr, respectively. At the start of the trajectory the distance from the gas atom to the nearest cluster atom equals the cut-off of the gas-Pd potential. Similarly, the trajectory is interrupted when the gas atom is more distant to any cluster atom than the cut-off distance. The total energy is conserved to at least 10^{-5} eV. In order to calculate the energy transfer averages that correspond to the desired temperatures $T_{\rm g}$, $T_{\rm trans}$ and $T_{\rm int}$, the initial gas and cluster atomic coordinates and velocities must be correctly distributed. In our earlier studies of the energy transfer [8–10] we performed similar simulations of

collisions between He and Pd_{13} and Pd_{55}, but the distributions were not correct. First, the cluster was initially rotationally and translationally frozen. Hence, the energy transfer to the cluster rotation and translation was always positive which is a problem when the gas and cluster temperatures are close. Second, the distribution of the relative speed of the gas atom and the cluster was based on infinite cluster mass. Third, the initial coordinate configuration of the cluster was extracted from a microcanonical ensemble and did only approximately represent the desired temperature. The error introduced in this way is generally small when a large cluster interacts with a small gas atom or molecule and the gas and cluster temperatures differ significantly. But the error is of importance in some of our present applications. Therefore, distribution functions without these approximations have been derived as presented in Appendix and used throughout the present study. In Appendix we find that the following parameters must be randomly generated in the selection of the starting point of the collision.

(i) The internal coordinates of the cluster atoms at the temperature $T_{\rm int}$ are generated by Monte Carlo simulations [11]. The cluster center of mass is placed in the origin.

(ii) The internal velocity in the x-direction of an atom in the cluster should be sampled according to

$$f\left(v_{x,j}\right) \propto \exp\left(-\frac{m_{\rm Pd} v_{x,j}^2}{2k_{\rm B}T_{\rm int}}\right), \qquad j = 1, ..., 13, \quad (10)$$

with a subsequent subtraction of the center of mass velocity. Here $m_{\rm Pd}$ is the mass of one palladium atom. Analogous sampling applies for the y- and z-directions. The set of internal velocities and the set of spatial configurations are combined to form a set of initial configurations of the cluster.

(iii) The probability density of the impact parameter should be given by

$$f_b\left(b\right) = \frac{2b}{b_{\rm max}^2}, \quad (11)$$

where $b_{\rm max}$ is the maximal impact parameter used in the simulations. In contrast we have used

$$\tilde{f}_b\left(b\right) = \begin{cases} 2\varsigma, & 0 < b < b_1 \\ \varsigma, & b_1 < b < b_{\rm max}. \\ 0, & b > b_{\rm max} \end{cases} \quad (12)$$

The value of ς is given by the normalization condition on $\tilde{f}_b\left(b\right)$. The reason for simulating relatively many trajectories with small b is that these trajectories contribute most significantly to the average energy transfer and the statistical accuracy is thereby enhanced. The correct average energy transfer will still be obtained since an appropriate weight factor will compensate for not using $f_b\left(b\right)$. The parameter $b_{\rm max}$ is chosen so that the interaction between the gas and the cluster is negligible if $b > b_{\rm max}$. We have used $b_{\rm max} = 12$, 12, 14 and 15 Å for the collisions with He, Ne, Ar and Kr, respectively. In all the collisions $b_1 = 8$ Å.

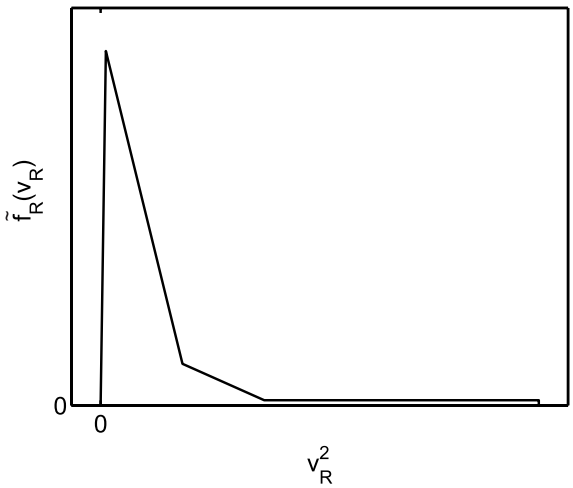

Fig. 2. The typical shape of $\tilde{f}_{\rm R}\left(v_{\rm R}\right)$ used in the simulations is shown.

The gas atom is placed so that the distance to the nearest palladium atom is equal to the cut-off of the corresponding Lennard-Jones potential. The collision is aborted when the rare gas atom again is out of the range of interaction from the cluster.

(iv) The relative speed between the gas and the cluster should be distributed according to

$$f_{\rm R}\left(v_{\rm R}\right) \propto v_{\rm R}^3 \exp\left(-\frac{\alpha v_{\rm R}^2}{2k_{\rm B}}\right), \quad (13)$$

where

$$\alpha = \frac{\dfrac{m_{\rm g}}{T_{\rm g}}\dfrac{m_{\rm c}}{T_{\rm trans}}}{\dfrac{m_{\rm g}}{T_{\rm g}} + \dfrac{m_{\rm c}}{T_{\rm trans}}}. \quad (14)$$

Here $m_{\rm g}$ and $m_{\rm c}$ are the gas mass and cluster mass, respectively. However, instead of using the temperature-dependent $f_{\rm R}\left(v_{\rm R}\right)$ for generation of $v_{\rm R}$ we have used a temperature-independent normalized function $\tilde{f}_{\rm R}\left(v_{\rm R}\right)$. The consequence is that $T_{\rm g}$ and $T_{\rm trans}$ need not be set before the simulations are run. Thus, the same set of simulations can be used for various $T_{\rm g}$ and $T_{\rm trans}$ and the saving of computational time is considerable. Again, a weight factor will compensate for not generating $v_{\rm R}$ according to $f_{\rm R}\left(v_{\rm R}\right)$. The choice of $\tilde{f}_{\rm R}\left(v_{\rm R}\right)$ is arbitrary but in order to obtain a small statistical error we have used a function that is a compromise between the distributions in equation (13) in the temperature intervals 100 K $< T_{\rm g} <$ 900 K and 100 K $< T_{\rm trans} <$ 1 100 K. For simplicity we let $\tilde{f}_{\rm R}\left(v_{\rm R}\right)$ be linear in $v_{\rm R}^2$ (see Fig. 2).

The energy transfer to the cluster as well as to the translational and internal degrees of freedom, respectively, can be calculated for the collision i as

$$\Delta E_{{\rm tot},i} = -\frac{m_{\rm g}}{2}\left(\left(\mathbf{v}_{{\rm g},i} + \Delta\mathbf{v}_{{\rm g},i}\right)^2 - \mathbf{v}_{{\rm g},i}^2\right) \quad (15)$$

$$\Delta E_{{\rm trans},i} = \frac{m_{\rm c}}{2}\left(\left(\mathbf{v}_{{\rm c},i} + \Delta\mathbf{v}_{{\rm c},i}\right)^2 - \mathbf{v}_{{\rm c},i}^2\right) \quad (16)$$

$$\Delta E_{{\rm int},i} = \Delta E_{{\rm tot},i} - \Delta E_{{\rm trans},i}. \quad (17)$$

Here $\mathbf{v}_c$ and $\mathbf{v}_g = \mathbf{v}_R + \mathbf{v}_c$ are the initial cluster (center of mass) translational velocity and the initial gas atom velocity, respectively, and $\Delta\mathbf{v}_c$ and $\Delta\mathbf{v}_g$ are the changes in $\mathbf{v}_c$ and $\mathbf{v}_g$ during the collision. The initial cluster translational velocity must be randomly generated too. Note that the generation of $\mathbf{v}_c$ is not needed for the simulation but only for the energy transfer calculation. Let us express this velocity as a sum of two components. One component is parallel and the other component is perpendicular to the relative velocity between gas and cluster,

$$\mathbf{v}_c = \mathbf{v}_{c_\parallel} + \mathbf{v}_{c_\perp}. \tag{18}$$

The distribution of the components is

$$f_{c_\parallel|R}\left(\mathbf{v}_{c_\parallel}|\mathbf{v}_R\right) \propto \exp\left(-\frac{\left(\mathbf{v}_{c_\parallel} + \delta\mathbf{v}_R\right)^2}{2\lambda^2}\right), \tag{19}$$

$$f_{c_\perp|R}\left(\mathbf{v}_{c_\perp}|\mathbf{v}_R\right) \propto \exp\left(-\frac{\mathbf{v}_{c_\perp}^2}{2\lambda^2}\right), \tag{20}$$

where

$$\delta = \frac{\dfrac{m_g}{T_g}}{\dfrac{m_g}{T_g} + \dfrac{m_c}{T_{trans}}} \tag{21}$$

and

$$\lambda = \sqrt{\frac{k_B}{\dfrac{m_g}{T_g} + \dfrac{m_c}{T_{trans}}}}. \tag{22}$$

An appropriate weight factor will make sure that the average energy transfer corresponds to the desired temperatures T_g, T_{trans} and T_{int}:

$$\langle\Delta E\rangle_{T_g,T_{trans},T_{int}} \approx \frac{\sum_i^N \Delta E_i g\left(b_i, v_{R,i}\right)}{\sum_i^N g\left(b_i, v_{R,i}\right)} \tag{23}$$

where

$$g\left(b, v_R\right) = \frac{f_b\left(b\right) f_R\left(v_R\right)}{\tilde{f}_b\left(b\right) \tilde{f}_R\left(v_R\right)}. \tag{24}$$

(See Appendix).

We are also going to study the energy transfer as a function of the impact parameter. The average energy transfer for the collisions with $b' < b < b''$ is

$$\langle\Delta E\rangle_{T_g,T_{trans},T_{int},b} \approx \frac{\sum_i^{N_b} \Delta E_i g\left(b_i, v_{R,i}\right)}{\sum_i^{N_b} g\left(b_i, v_{R,i}\right)}, \tag{25}$$

where only the N_b collisions with $b' < b < b''$ are included in the sums.

4.2 Model potentials

The interaction between the atoms in the cluster is described by the Many-Body Alloy potential, developed by Tománek and co-workers [26]. The potential energy of the cluster is written as a sum of the cohesive energies of all atoms in the cluster

$$U\left(\mathbf{R}\right) = \sum_{j=1}^{N} U_j, \tag{26}$$

where

$$U_j = -\xi_0 \sqrt{\sum_{k\neq j} \exp\left(-2q\left(r_{jk}/r_0 - 1\right)\right)} + \epsilon_0 \sum_{k\neq j} \exp\left(-p\left(r_{jk}/r_0 - 1\right)\right). \tag{27}$$

Here r_{jk} is the distance between atoms j and k. The repulsive part of the binding energy is of pairwise Born-Mayer type. In the attraction, many-body character is included by a tight-binding second-moment approximation of the d band density of states. We have used the parameters that were calculated by fitting the energy to LDA calculations of the minimal energy structure of bulk palladium [26]. The parameter values are $\xi_0 = 1.2630$ eV, $\epsilon_0 = 0.08376$ eV, $r_0 = 2.758$ Å, $p = 14.8$ and $q = 3.40$. The same parameters have been used in our previous publications on cluster cooling [8–10] and in the heat capacity calculation and initial cluster configuration generation [11].

For the interaction between one cluster atom and the rare gas atom we have used the Lennard-Jones potential

$$U_{LJ}\left(r_j\right) = 4\epsilon\left(\left(\frac{\sigma}{r_j}\right)^{12} - \left(\frac{\sigma}{r_j}\right)^{6}\right), \qquad j = 1, ..., 13, \tag{28}$$

where r_j is the distance between the gas atom and cluster atom number j. The interaction between the gas atom and one palladium atom is approximated by replacing palladium with the next larger rare gas atom, namely xenon. Then the Lorentz-Berthelot rules are applied. According to the these rules [27] the Lennard-Jones parameters for He–Xe are

$$\sigma_{He-Xe} = (\sigma_{He-He} + \sigma_{Xe-Xe})/2 = (2.58\text{ Å} + 4.06\text{ Å})/2 = 3.32\text{ Å} \tag{29}$$

$$\epsilon_{He-Xe} = \sqrt{\epsilon_{He-He}\epsilon_{Xe-Xe}} = \sqrt{0.88 \times 19.7}\text{ meV} = 4.2\text{ meV}. \tag{30}$$

The parameters for Ne–Xe, Ar–Xe and Kr–Xe are calculated analogously giving $\sigma = 3.425$, 3.74, 3.835 Å and $\epsilon = 7.8$, 14.5, 18.0 meV, respectively. The original Lennard-Jones parameters are taken from reference [28]. As Lennard-Jones cut-off distance we have used 8, 9, 10 and 12 Å for He, Ne, Ar, and Kr, respectively.

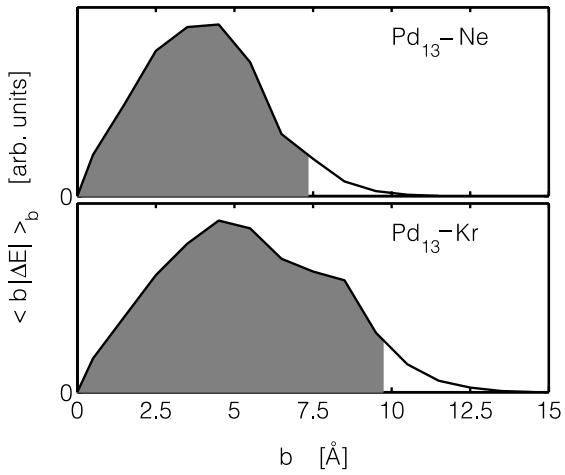

Fig. 3. $\langle b\,|\Delta E|\rangle_b$ *versus* b is shown for collisions with Kr and Ne. Gas and cluster temperatures are 700 K. The shaded areas show 95% of the total areas.

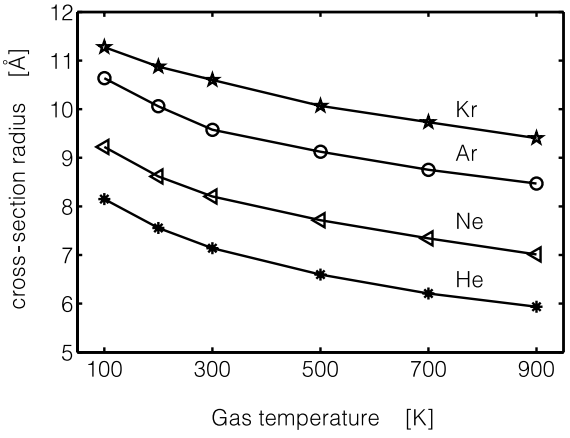

Fig. 4. The collision cross-section radius, *csr*, *versus* gas temperature in collisions with He (stars), Ne (triangles), Ar (rings) and Kr (pentagrams) is shown. The temperature of Pd_{13} is 700 K.

5 The collision frequency and cross-section

Since the energy transfer is from a mathematical point of view non-zero for any impact parameter when using classical mechanics, the separation between hits and misses is arbitrary in simulations. The average energy transfer depends on what gas atom trajectories we regard as hits and which ones we regard as misses. The larger the cross-section is, the smaller is the average energy transfer. A normal procedure to estimate a cross-section is to study the energy transfer *versus* b [29]. In Section 6.2 (Fig. 8) we will find that when the cluster and gas are near equilibrium, the plot of $\langle \Delta E\rangle_b$ will change from positive to negative to zero with increasing b. This behavior makes plots of $\langle \Delta E\rangle_b$ *versus* b unsuitable for cross-section estimations when $T_g \approx T_c$. Instead we have used the curve $\langle b\,|\Delta E|\rangle_b$ *versus* b for cross-section estimation (see Fig. 3). The energy transfer, regardless of sign, is a measure of the interaction between the gas and the cluster and $\langle b\,|\Delta E|\rangle_b$ will naturally always be positive and it shows a tail for large b. The cross-section radius, $csr = \sqrt{\text{cross-section}\ /\pi}$, of the collisions we define by

$$\frac{\int_0^{csr} \langle b\,|\Delta E|\rangle_b \,\mathrm{d}b}{\int_0^{\infty} \langle b\,|\Delta E|\rangle_b \,\mathrm{d}b} = 0.95. \qquad (31)$$

The choice of 0.95 as the limit is of course arbitrary. The cross-section radius varies only a few percent with cluster temperature but is more sensitive to the gas temperature. In Figure 4, *csr* at $T_c = 700$ K is drawn for various gas temperatures and different gases. The cross-section radius increases significantly with decreasing gas temperature. This result is not surprising. When the gas temperature is low, *i.e.* the gas speed is on average low, the attraction of the potential can capture gas atoms for far larger impact parameters than for high T_g.

The cross-sections in Figure 4 vary considerably between the different rare gases but the differences are almost independent of gas temperature. However, the cross-section radii do not compare favorably with those predicted by the formula for the geometric cross-section radii proposed by Leopold *et al.* [30],

$$csr = \underbrace{r_{\mathrm{Pd}} n^{1/3} + \delta_{\mathrm{spill-out}}}_{\text{cluster radius}} + \underbrace{r_{\mathrm{gas}}}_{\text{gas atom radius}}. \qquad (32)$$

Here r_{Pd} is the Wigner-Seitz radius of a palladium atom, n is the number of atoms in the cluster, $\delta_{\mathrm{spill-out}}$ is an empirical constant to account for electron spill-out and r_{gas} is the rare gas atom radius. For r_{gas} we have used $2^{1/6}\sigma_{\mathrm{gas-gas}}/2$ which is the minimum energy distance in a Lennard-Jones dimer. We find the literature values $r_{\mathrm{Pd}} = 1.52$ Å [31] and $\sigma = 2.58$, 2.79, 3.42 and 3.61 Å for He, Ne, Ar and Kr, respectively [28]. Leopold *et al.* [30] used the value $\delta_{\mathrm{spill-out}} = 0.5$ Å which would yield the cross-section radii 5.5, 5.6, 6.0 and 6.1 Å for Pd_{13}–He, Pd_{13}–Ne, Pd_{13}–Ar and Pd_{13}–Kr, respectively. Our definition in equation (31) above suggests a considerably larger increase of *csr* with increasing gas atom size. The curves of $\langle b\,|\Delta E|\rangle_b$ *versus* b in Figure 3 are similar in shape for the Pd_{13}–Ne and Pd_{13}–Kr collisions. Thus we regard our definition of the cross-section to be suitable for our application of comparing the energy transfer efficiency but care should be taken when using the estimated cross-section radius in other applications.

The average energy transfer taken over all collisions with $b < b_{\max}$ we denote $\langle \Delta E\rangle_{T_g,T_c,b_{\max}}$. If $b_{\max}$ is increased, $\langle \Delta E\rangle_{T_g,T_c,b_{\max}}$ will decrease according to [8]

$$\lim_{b_{\max}\to\infty} \langle \Delta E\rangle_{T_g,T_c,b_{\max}}\, b_{\max}^2 = \text{constant}. \qquad (33)$$

The average energy transfer that corresponds to the reasonable cross-section radius estimated using equation (31)

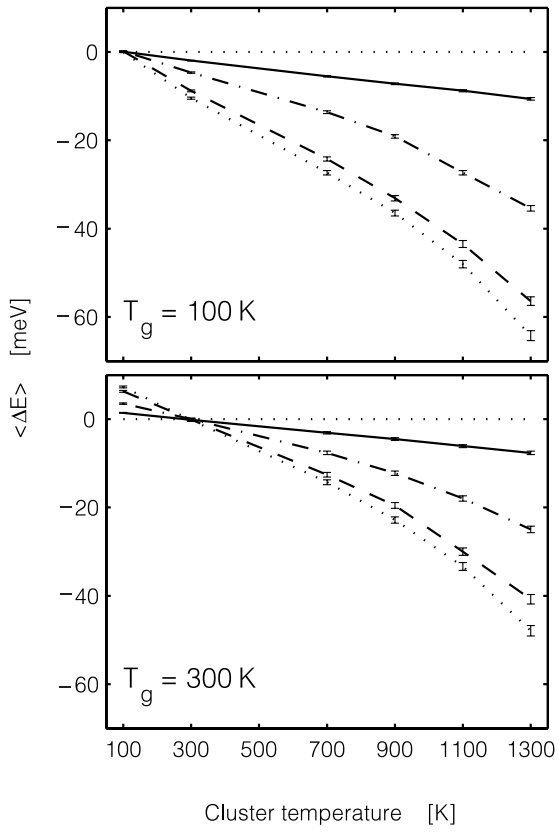

Fig. 5. The average energy transfer to Pd_{13} in collisions with He (solid line), Ne (dashed-dotted), Ar (dashed) and Kr (dotted), respectively, is shown. The energy transfer is rescaled according to equation (33). The errorbars shown are the statistical error in the form of 95% confidence intervals. (Top panel) The gas temperature is 100 K. The cross-section radii used are 8.2 Å (He), 9.2 Å (Ne), 10.4 Å (Ar) and 11.4 Å (Kr). (Bottom panel) The gas temperature is 300 K. The cross-section radii used are 7.2 Å (He), 8.3 Å (Ne), 9.5 Å (Ar) and 10.5 Å (Kr).

can be calculated by

$$\langle \Delta E \rangle_{T_\mathrm{g},T_\mathrm{c}} = \frac{\langle \Delta E \rangle_{T_\mathrm{g},T_\mathrm{c},b_\mathrm{max}} \pi b_\mathrm{max}^2}{\pi csr^2} \cdot \tag{34}$$

Although the cross-section radius is in reality slightly dependent on the cluster temperature we have used the same radius for all cluster temperatures. The cross-section radii that we have used in Figure 5 are for He 8.2 Å (T_g = 100 K) and 7.2 Å (T_g = 300 K). For Ne we have used 9.2 Å and 8.3 Å, for Ar 10.4 Å and 9.5 Å and for Kr 11.4 Å and 10.5 Å at T_g = 100 and 300 K, respectively. The energy transfer averages in Figure 7 are rescaled to the cross-section radii in Figure 4.

The rescaling of the average energy transfer to the reasonable cross-section radii is necessary when the energy transfer efficiency is compared between different colliding species. In contrast, in the cooling equation (Eq. (5)) the nonuniqueness in the choice of cross-section is fortunately without consequence. The reason is that $\langle \Delta E \rangle_{T_\mathrm{g},T_\mathrm{c}}$ is inversely proportional to csr^2 but the collision frequency is proportional to csr^2 and the cross-section dependencies therefore cancel each other.

The collision frequency between a *single* cluster and all gas atoms in a gas mixture when $T_\mathrm{trans} = T_\mathrm{g}$ is obtained by a well-known expression

$$z = \pi csr^2 \frac{P_\mathrm{g}}{T_\mathrm{g}} \sqrt{\frac{8}{\pi k_\mathrm{B} \mu / T_\mathrm{g}}} \tag{35}$$

(see *e.g.* Ref. [32]). The rare gas is ideal at the low pressure P_g and μ is the reduced mass,

$$\mu = \frac{m_\mathrm{g} m_\mathrm{c}}{m_\mathrm{g} + m_\mathrm{c}} \cdot \tag{36}$$

In the cooling equation, however, the collision frequency is required between gas atoms and one cluster when $T_\mathrm{g} \neq T_\mathrm{trans}$. The collision frequency depends on the distribution of the relative speed of the colliding particles. The distribution is determined by the parameter μ/T when the gas and the cluster are in equilibrium, but by α (Eq. (14)) when the translational temperatures differ. Thus, in this case the collision frequency is

$$z\left(T_\mathrm{trans}, T_\mathrm{g}, P_\mathrm{g}\right) = \pi csr^2 \frac{P_\mathrm{g}}{T_\mathrm{g}} \sqrt{\frac{8}{\pi k_\mathrm{B} \alpha\left(T_\mathrm{trans}, T_\mathrm{g}\right)}} \cdot \tag{37}$$

Equation (5) may now be rewritten as

$$\begin{aligned} \mathrm{d}T_\mathrm{trans} &= \frac{\langle \Delta E_\mathrm{trans} \rangle_{T_\mathrm{g},T_\mathrm{trans},T_\mathrm{int}} z\left(T_\mathrm{trans}, T_\mathrm{g}\right)}{c_\mathrm{trans}\left(T_\mathrm{trans}\right)} \mathrm{d}t \\ &= \frac{1}{T_\mathrm{g}} \sqrt{\frac{8}{\pi k_\mathrm{B} \alpha\left(T_\mathrm{trans}, T_\mathrm{g}\right)}} \frac{\langle \Delta E_\mathrm{trans} \rangle_{T_\mathrm{g},T_\mathrm{trans},T_\mathrm{int}} \pi csr^2}{c_\mathrm{trans}\left(T_\mathrm{trans}\right)} P_\mathrm{g} \mathrm{d}t. \end{aligned} \tag{38}$$

There is no dependence on csr in the last expression in equation (38). All the parameters and functions except the pressure of the rare gas are known. The pressure is however only a constant that rescales the time. The cooling equation is analogous for the internal temperature

$$\begin{aligned} \mathrm{d}T_\mathrm{int} = \frac{1}{T_\mathrm{g}} \sqrt{\frac{8}{\pi k_\mathrm{B} \alpha\left(T_\mathrm{trans}, T_\mathrm{g}\right)}} \\ \times \frac{\langle \Delta E_\mathrm{int} \rangle_{T_\mathrm{g},T_\mathrm{trans},T_\mathrm{int}} \pi csr^2}{c_\mathrm{int}\left(T_\mathrm{int}\right)} P_\mathrm{g} \mathrm{d}t. \end{aligned} \tag{39}$$

6 Results

6.1 Energy transfer results

In Figure 5, the average total energy transfer to the cluster is drawn for the gas temperatures 100 K and 300 K, respectively, and the cluster temperatures from 100 to 1 300 K. The averages are based on N = 45 000 simulated collisions for each pair of rare gas and cluster temperature. The figure shows that the energy transfer is zero

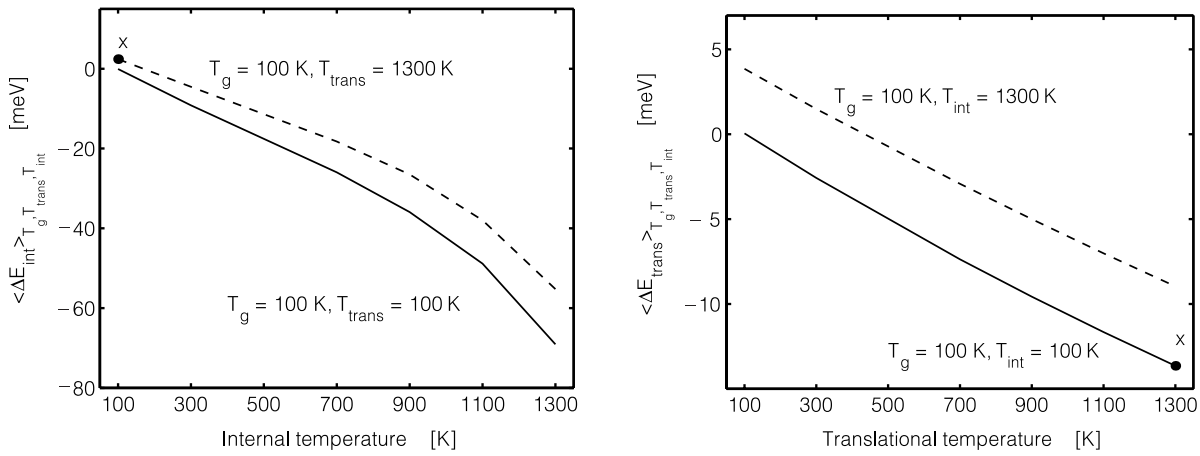

Fig. 6. (a) The average energy transfer to the internal degrees of freedom of the cluster in collisions with Kr is shown as a function of internal temperature. The translational temperature is 100 K (solid line) and 1 300 K (dashed line). The temperature of the krypton gas is 100 K. (b) The average energy transfer to the translation of the cluster is shown as a function of translational temperature. The internal temperature is 100 K (solid line) and 1 300 K (dashed line). The temperature of the krypton gas is 100 K.

when $T_g = T_c$, as required. At low cluster temperatures the energy transfer is almost linear in $(T_g - T_c)$, but at higher T_c the energy transfer is more efficient. One reason is that Pd_{13} starts to melt at about 900 K [11] and the energy transfer to the molten cluster is more efficient. Moreover, the curves show that the energy transfer efficiency increases with gas atom size but that the difference in efficiency between argon and krypton is relatively small. In general, the heavier and slower gas atoms have more time to interact with the cluster which causes an increase in the energy transfer.

The same set of collision simulations of $Pd_{13}-Kr$ as in Figure 5 are used to calculate $\langle \Delta E_{trans} \rangle_{T_g, T_{trans}, T_{int}}$ when T_{int} = 100 K and 1 300 K, respectively and $\langle \Delta E_{int} \rangle_{T_g, T_{trans}, T_{int}}$ when T_{trans} = 100 K and 1300 K, respectively. The gas temperature is 100 K. The results are drawn in Figure 6. The curves show that, in the collisions, energy is redistributed within the cluster when $T_{trans} \neq T_{int}$. For instance, at point x in Figure 6, T_{trans} = 1 300 K and $T_g = T_{int}$ = 100 K and the internal degrees of freedom are warmed and the translation is cooled more than if T_{int} had been 1300 K.

6.2 The characteristics of collision trajectories at various impact parameters

Let us now investigate the collisions in depth. At the cluster temperature 700 K, 45 000 collisions were simulated for each of the cases $Pd_{13}-Ne$ and $Pd_{13}-Kr$ and the energy transfer of the different modes of motion was calculated for gas temperatures from 100 K to 900 K. The result is shown in Figure 7. Note that the abscissa is now the gas temperature. First we see that the average energy transfer is zero to the translational and internal degrees of freedom

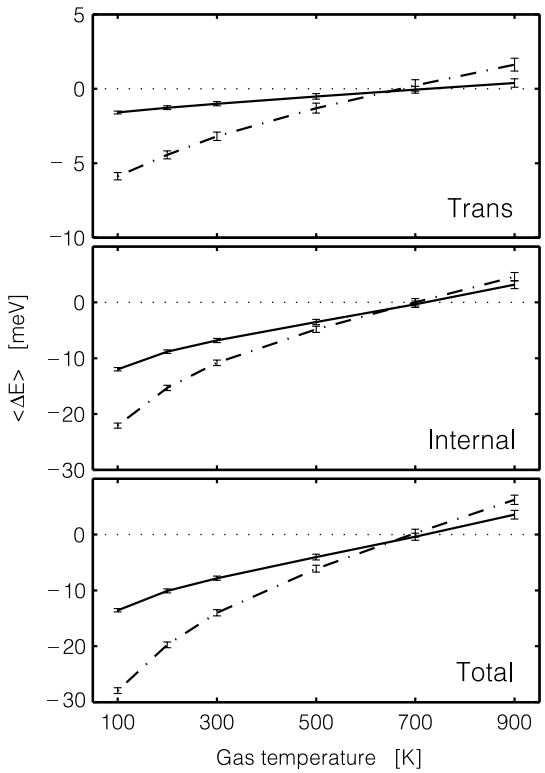

Fig. 7. The average energy transfer *versus* gas temperature is shown for 45 000 collisions between Ne and Pd_{13} (solid lines) and Kr and Pd_{13} (dashed-dotted lines). The cluster temperature is 700 K. The energy transfer is to the translational modes (top panel), internal modes (middle) and all modes (bottom) of the cluster. The energy transfer is rescaled according to equation (33) using the cross-section radii in Figure 4. The errorbars shown are the statistical errors in the form of 95% confidence intervals.

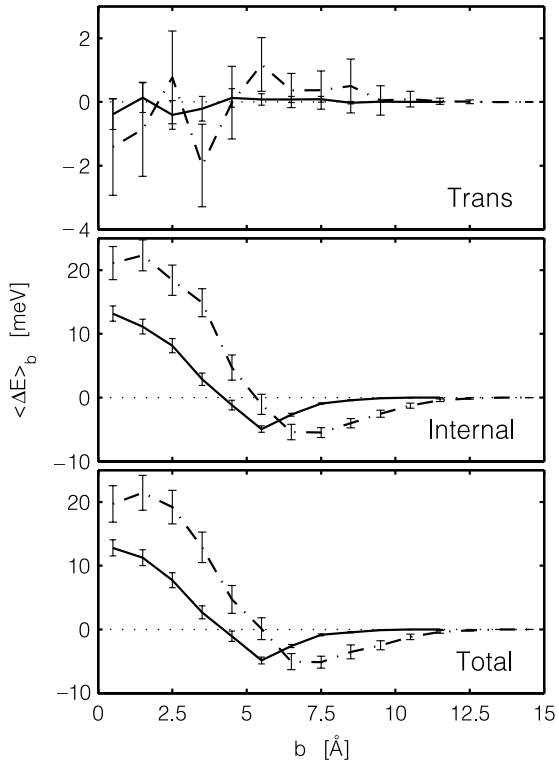

Fig. 8. The average energy transfer *versus* the impact parameter in 135 000 collisions between Ne and Pd_{13} (solid lines) and 45 000 collisions between Kr and Pd_{13} (dashed-dotted lines) is shown for $T_g = T_c$ =700 K. The energy transfer is to the translational modes (top panel), internal modes (middle) and all modes (bottom) of the cluster. The errorbars shown are the statistical errors in the form of 95% confidence intervals.

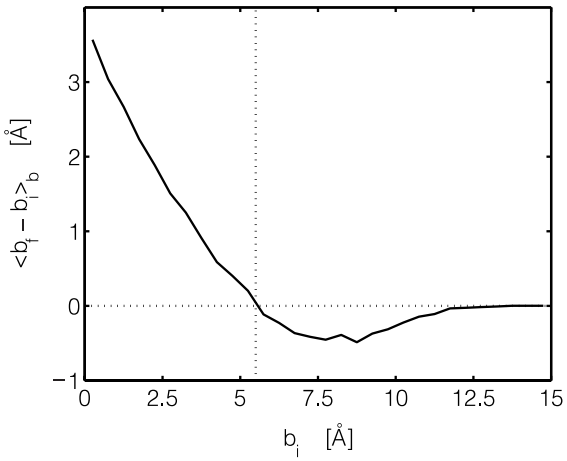

Fig. 9. The average change in b *versus* the initial b in 45 000 collisions between Kr and Pd_{13} is shown for $T_g = T_c$ =700 K. The vertical dotted line indicates the hard core radius of the cluster.

as well as to the whole cluster when $T_c = T_g$. The curves seem linear at high gas temperatures but at low T_g the energy transfer efficiency increases. This enhanced energy transfer can be explained by the fact that the gas atom is captured by the attraction of the cluster and multiple encounters occur for each collision. We will return to this phenomenon in a subsequent publication.

Since each collision trajectory can be studied in simulations, the dependence of various properties on the impact parameter can be investigated. However, the outcome of one trajectory at a specific b is so variable that it is mainly the average behavior of a large number of trajectories that is of interest.

In Figure 8 the energy transfer at $T_g = T_c = 700$ K is drawn *versus* b. The figures show that equilibrium does not necessarily imply that the energy transfer is zero for all b. Instead it seems that collisions with a small impact parameter heat the cluster but collisions with larger b cool the cluster. In the special case of translational energy the curves indicate that the energy transfer is zero for all b. The errorbars are however large for Kr. In order to reduce the errorbars, more collisions were simulated for Pd_{13}−Ne so that the curves in Figure 8 represent 135 000 collisions. The curve for neon is so close to zero that we believe that it is generally true that the energy transfer to the translational mode vanishes for all b. This is in accord with the collisions between the hard spheres, where only the translational mode is present (see Appendix and Fig. 16).

One of the fundamental tests of simulation results is that they should be time reversal invariant. The curves in Figure 8 show that collisions with a small initial b on average heat the cluster. If all the collisions were simulated time reversed, heating trajectories would turn into cooling trajectories. But since heating trajectories on average should start at large b we find that in order to satisfy time reversibility, collisions with small initial b must on average end with a large b and *vice versa.* In Figure 9, the average change of impact parameter, $\langle b_{\text{final}} - b_{\text{initial}} \rangle_b$, is drawn *versus* b for the collisions Pd_{13}−Kr at $T_g = T_c = 700$ K. Indeed, the change in b is confirmed. The zero change is obtained when $b = 5.6$ Å which is approximately the same point as where the total energy transfer turns negative ($b = 5.5$ Å). The vertical dotted curve indicates the inner-most radius where the force between Pd_{13} and Kr changes from attractive to repulsive at $T_c = 0$ K. This radius, 5.5 Å, can be regarded a hard core radius of the cluster and it approximately coincides with the change from positive to negative $\langle b_{\text{final}} - b_{\text{initial}} \rangle_b$.

By studying whether the gas atom is overall attracted or repelled by the cluster, the trajectories can be divided into two classes. The average angle ϕ between the final and the initial gas velocity is calculated for the Pd_{13}−Kr collisions at $T_g = T_c = 700$ K. The curve is shown in Figure 10. For small b the collisions result in a bouncing back such that ϕ is on average 140°. The reflection gradually decreases and with very large b, the gas atom passes by without notice and the angle is zero. Let us now assign a sign to the angles. If the net effect by the cluster is a bending of the gas trajectory towards the cluster, the angle is defined to be positive, otherwise it is negative (see the inset in Fig. 10). The average of these angles is denoted ϕ_s. At $b = 0$ Å, the gas atom might bounce in any

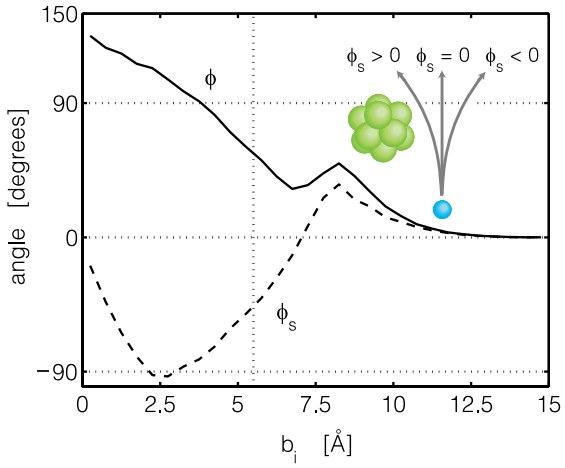

Fig. 10. The average change in angle of the gas atom velocity *versus* the initial b in 45 000 collisions between Kr and Pd_{13} is shown for $T_g = T_c = 700$ K. The solid line shows the change when all angles are regarded as positive. In the inset the definition of positive and negative angle changes is illustrated. The dashed curve shows the change of angle including sign. The vertical dotted line indicates hard core radius of the cluster.

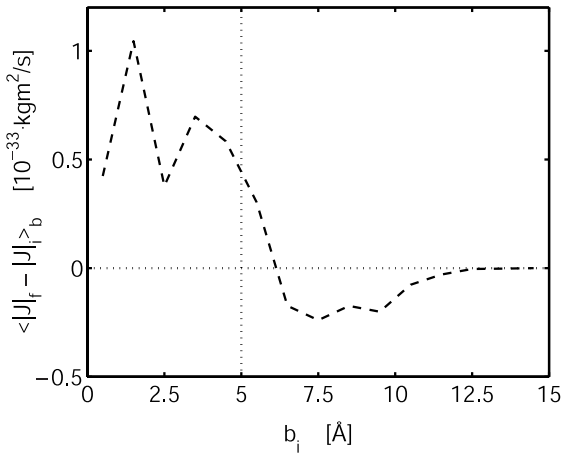

Fig. 11. The average change of the norm of the angular momentum is shown *versus* the initial b in 45 000 collisions between Kr and Pd_{13} for $T_g = T_c = 700$ K. The vertical dotted line indicates the hard core radius of the cluster.

direction and the average angle inclusive sign is zero. For $b = 2.5$ Å, a clear bounce away from the cluster can be seen. In contrast, for large b, the average angle is positive. In such trajectories, the gas atom is attracted by the cluster but it never collides with the hard core of the cluster. The change from negative to positive angles occurs at $b = 7.1$ Å. Figures 9 and 10 are in agreement. When the initial b is small, the gas atom bounces off the rough cluster surface and it is unlikely that it will leave the cluster with the same small b. However, for larger impact parameters, a net attraction is experienced by the gas atom and it leaves with a smaller b than the initial one.

The angular momentum $J = |\mathbf{J}|$ of the cluster exhibits the same b-variation. In the Pd_{13}−Kr collisions at $T_g = T_c = 700$ K, the net change in J is zero. However, the average change in J in a collision is positive for small b and negative for $b > 6.2$ Å (see Fig. 11). As the cluster is solid at 700 K [11], and hence the moment of inertia is almost unaltered during the collision, an increase in J is also an increase in the rotational energy.

In the trajectories with a larger impact parameter, the net attraction of gas atom is certainly one of the reasons why the final b is smaller. It is however not the only reason. Simulations were performed with the Lennard-Jones potential turned into a hard sphere potential. The intracluster potential was unaltered. In such simulations, trajectories with a large b ended on average with a smaller b, although the gas atom was not attracted by the cluster. Similarly, the energy transfer was positive for small b, but negative to the same extent for larger b at $T_g = T_c = 700$ K. Hence the reason for the b variation is also an effect due to the inherent nature of scattering in the collisions.

6.3 Solution of the cooling equation

The cooling equation was solved for the different rare gases and the result is shown in Figure 12. The initial cluster temperature was 1 300 K and the gas pressure was 100 mbar. Note that the pressure only serves to define the timescale of the cooling while our simulations are done as to reflect behavior in the low gas density limit. Near equilibrium the temperature of the clusters will decay approximately exponentially and the cooling cannot reach exactly $T_c = T_g$ in finite time. Therefore, in order to calculate a finite time required to cool the clusters, the cooling must be regarded as complete when the clusters are at a temperature, T_{cool}, higher than the gas temperature, T_g. The limit T_{cool} may be defined arbitrarily in these calculations.

In an ensemble of Pd_{13} clusters at the temperature T the average and standard deviation of the kinetic energy are

$$\langle E_{kin} \rangle_T = 3n/2 k_B T \tag{40}$$

and

$$\sigma_{E_{kin},T} = \sqrt{3n/2} k_B T. \tag{41}$$

We have chosen to define T_{cool} by

$$\langle E_{kin} \rangle_{T_{cool}} = \langle E_{kin} \rangle_{T_g} + \sigma_{E_{kin},T_g}. \tag{42}$$

Given that $n = 13$ we obtain $T_{cool} = 1.23 T_g$. Hence, in the calculations at $T_g = 100$ K and 300 K we consider the clusters to be in "preequilibrium" and completely cooled at 123 K and 369 K, respectively. The curves in Figure 12 terminate at the time when these temperatures are reached. The times, t_{cool}, required to cool the cluster to T_{cool} are listed in column three in Table 1.

The cooling of the translational temperature is indeed much faster than the cooling of internal modes for all gases. Furthermore we can see that the cooling to 100 K is faster than the cooling to 300 K. The reason is that the energy transfer efficiency is greater at $T_g = 100$ K than at $T_g = 300$ K. This in turn is due to the fact that when the

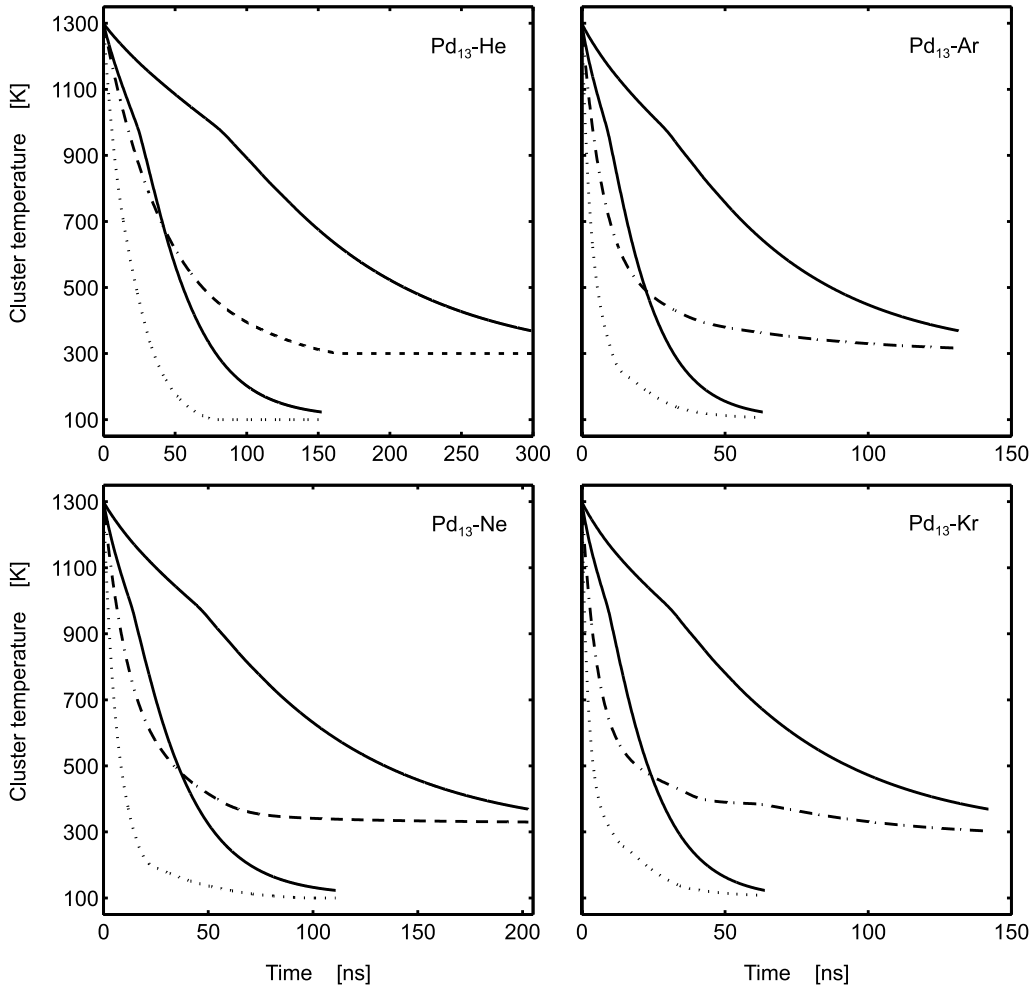

Fig. 12. The temperature decay of a Pd_{13} cluster in a rare gas atmosphere of 100 mbar is shown. The initial cluster temperature is 1 300 K and the cooling is considered as complete when the internal temperature has reached 123 K and 369 K, respectively. The solid curves show the internal temperature and the dashed/dotted ones show the translational temperature. N.B. The time scales are different for the different gases.

Table 1. The table lists the time required to cool the cluster to "preequilibrium", $t_{\rm cool}$, and halftimes, τ, for the cooling of Pd_{13} in collisions with the rare gas atoms. The calculations refer to the internal degrees of freedom of the cluster. The initial cluster temperature is 1 300 K and the gas pressure is 100 mbar.

Colliding species	$T_{\rm g}$ (K)	$t_{\rm cool}$ (ns)	τ (ns)
Pd_{13}−He	100	152	34
Pd_{13}−Ne	100	111	27
Pd_{13}−Ar	100	63	14
Pd_{13}−Kr	100	64	14
Pd_{13}−He	300	299	88
Pd_{13}−Ne	300	203	65
Pd_{13}−Ar	300	132	43
Pd_{13}−Kr	300	142	47

gas is very cold the duration of the collision is increased and sometimes the gas atom is even captured, making multiple encounters before leaving the cluster. With a longer collision time, the colliding species have more time to exchange energy.

For all gases the cooling rate has a minimum when the internal temperature is about 1 000 K. The reason is that the cluster is about to change from molten to solid phase and energy must be removed for the transition to take place.

In collision simulations it is common to assume that the translational temperatures of the colliding species reach equilibrium so quickly that the translation can be assumed to be equilibrated from the start. Such an assumption can be tested in our simulations. By forcing $T_{\rm trans} = T_{\rm g}$ throughout the cooling, the internal temperature can be followed under this assumption. The resulting curves of the internal temperature *versus* time are so similar to the curves in Figure 12, that they are not distinguishable. The maximal difference in temperature at any time is about 10 K. Hence we can conclude that the assumption of immediate equilibration of the translation is acceptable.

After the cluster has been cooled to solid phase the temperature of the internal degrees of freedom decays almost exponentially as

$$T_{\rm int}\,(t) = T_{\rm g} + \text{constant} \times \exp\left(-t \ln 2/\tau\right). \qquad (43)$$

In a lin-log plot the decay appears linear and the halftime τ may be identified from the slope. The halftimes for the cooling of the internal degrees of freedom of the

cluster with the different gases are presented in column four in Table 1.

Both $t_{\rm cool}$ and τ show that argon qualifies as the most efficient cooling agent being, however, only slightly better than krypton. Neon is less efficient and helium is the least efficient cooling agent. The reason argon can cool the cluster faster than krypton even though the energy transfer is better in collisions with krypton, is that the collision frequency is higher for argon than for krypton.

7 Conclusion

The cooling of Pd_{13} in collisions with rare gas atoms have been studied using a system of coupled differential equations describing the temperature decay of the translational and internal degrees of freedom of the cluster. The temperature-dependent properties that determine the decay are the heat capacity of the cluster, the collision frequency and the energy transfer in the gas-cluster collisions. An analytical expression is used for the collision frequency but the heat capacity and the energy transfer were obtained by means of simulation. The heat capacity was calculated in a previous work [11]. The energy transfer has been calculated by means of molecular dynamics simulation.

Distributions of the initial coordinates and velocities have been derived and a simulation scheme is presented (see Appendix) which leads to a correct zero energy transfer when the temperatures of the colliding species are equal. The average energy transfer of all modes in the collisions with Pd_{13} is an almost linear function of the temperature difference $T_{\rm g} - T_{\rm c}$ except at low gas temperature where the energy transfer is more efficient due to multiple encounters.

The collisions are also investigated for different impact parameters when the colliding species are in thermal equilibrium. From calculations for hard spheres (see Appendix) and from the simulation results for $Pd_{13}-Ne$ collisions we draw the conclusion that the translational energy transfer is zero for all b. The trajectories can however be divided into two classes with b less than or greater than about 5.5 Å in the case of Kr. In collisions with smaller b the gas atom bounces off the cluster and the gas atom typically leaves with a larger b then the initial b. In general, these trajectories heat the cluster and excite the cluster angular momentum. The trajectories with larger b are on average attracted by the cluster and the gas atom does not experience any hard collision. In such trajectories, the gas atom is heated and the angular momentum of the cluster is cooled. Furthermore, in such simulations, the final impact parameter is on average smaller than the initial one. The reason for this behavior is not exclusively the attraction of the cluster, since the same phenomenon is observed when the cluster-gas attraction is turned off.

The energy transfer *versus* b is not in full accord with what others have observed [29,33–35]. In these earlier publications, the energy transfer never changed sign as a function of b. We suppose the reason is that in these earlier simulations, the difference in temperature of the colliding species was so large that energy transfer was either all positive or all negative. Indeed, that is what we have observed when the species are far from equilibrium. The interesting sign change in $\langle \Delta E \rangle_b$ that we have found is confined to a small range of similar gas and cluster temperatures.

When cooling the cluster, we have observed that the cluster translation is cooled considerably faster than are the internal degrees of freedom. The energy transfer to the cluster must therefore be calculated in the case when $T_{\rm trans}$ and $T_{\rm int}$ differ. In this case the calculations show that in collisions an energy redistribution occurs in the cluster bringing it towards translational-internal equilibrium. The difficulty associated with determination of a proper cross-section, involved in for instance, energy transfer efficiency calculations [29], disappears in the cooling equation as the dependence on the cross-section in both the energy transfer and the collision frequency cancel.

The temperature decay shows first a shoulder due to the phase transition from molten to solid cluster phase, and then an approximately exponential decay. Figure 5 shows that when the mass of the gas atom and the gas-cluster potential depth increase, so does the energy transfer. In a previous publication we saw that both these gas properties contribute to a greater energy transfer efficiency [8]. Due to the factor $1/\sqrt{\alpha}$ in the collision frequency argon, which is lighter, becomes a better cooling agent than krypton. The difference is however small.

By implementing the condition that $T_{\rm trans} = T_{\rm g}$ throughout the cooling, we have tested the often used assumption that the translation is instantaneously equilibrated with the gas on the time-scale of internal equilibration. The change in internal temperature decay caused by this constraint was almost invisible and our calculations therefore confirm the accuracy of the usual assumption of thermalized translation.

The simulation sampling scheme has proven to be very convenient since the average energy transfer can be calculated for various $T_{\rm g}$ and $T_{\rm trans}$, using the same set of simulations. The selected temperatures then appear in weighting factors applied to each simulation as it appears in an ensemble average or distribution. We note, however, that such a reweighting scheme will not apply in its present simple form in the case when colliding molecules have internal degrees of freedom.

We thank Dr Nikola Marcovic at the Department of Physical Chemistry, Chalmers University of Technology, for very fruitful discussions. The project was financed by the The Swedish Natural Science Research Council, NFR.

Appendix A: Energy transfer in binary collisions

A.1. Colliding hard spheres

A.1.1. Collisions in a one-dimensional space

The derivation of the distribution functions of the initial velocities and coordinates that should be used in the

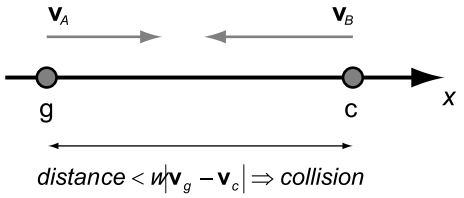

Fig. 13. A particle c with the velocity $\mathbf{v}_\mathrm{c}$ will collide with the particle g with the velocity $\mathbf{v}_\mathrm{g}$ if the distance between g and c is less than $w\left|\mathbf{v}_\mathrm{g}-\mathbf{v}_\mathrm{c}\right|$.

simulations will be illustrated on colliding hard spheres in one and three dimensions. Collisions between hard spheres do not require simulation as the change in momenta of the species is analytically obtainable. Say that a gas consists of a homogeneous mixture of hard sphere particles g and c. The particles are constrained to move in one dimension along an axis x. Since the only form of energy of a hard sphere is the kinetic energy, the energy transfer to particle c is

$$\Delta E = \frac{m_\mathrm{c}}{2}\left(\left(\mathbf{v}_\mathrm{c}+\Delta\mathbf{v}_\mathrm{c}\right)^2-\mathbf{v}_\mathrm{c}^2\right), \tag{44}$$

where m_c is the mass and $\mathbf{v}_\mathrm{c}$ is the initial velocity of particle c. The velocity change of particle c in the collision is $\Delta\mathbf{v}_\mathrm{c}$. Since the total momentum and the total kinetic energy must be conserved in a collision, $\Delta\mathbf{v}_\mathrm{c}$ is

$$\Delta\mathbf{v}_\mathrm{c} = \frac{2\left(\mathbf{v}_\mathrm{g}-\mathbf{v}_\mathrm{c}\right)}{1+m_\mathrm{c}/m_\mathrm{g}}, \tag{45}$$

where m_g is the mass and $\mathbf{v}_\mathrm{g}$ is the initial velocity of particle g. We now assume that all the particles g along the x-axis are in equilibrium at the temperature T_g and that the particles c are at temperature T_c. What is the average energy transfer to particles c? In order to calculate this average, the probability distribution $f_\mathrm{gc}\left(\mathbf{v}_\mathrm{g},\mathbf{v}_\mathrm{c}\right)$ of initial velocities in a collision must be derived.

Let us pick one particle g with velocity $\mathbf{v}_\mathrm{g}$ and calculate how many times during the time w it will collide with particles c with velocity $\mathbf{v}_\mathrm{c}$. For simplicity, g is assumed to be located at the origin. At first, consider the case in Figure 13: g is to the left of c, and g is moving to the right. The particle g will collide with all particles c that initially are in the x interval $[0, w\left(\mathbf{v}_\mathrm{g}-\mathbf{v}_\mathrm{c}\right)]$. If c moves to the right with a higher speed than g, the particles c that are to the left of g, in the interval $\left[w\left(\mathbf{v}_\mathrm{g}-\mathbf{v}_\mathrm{c}\right),0\right]$ will collide with g. Since the particles c are homogeneously spread over the x-axis, the number of collisions must be proportional to $w\left|\mathbf{v}_\mathrm{g}-\mathbf{v}_\mathrm{c}\right|$. The situation when g is moving to the left is analogous and we find that $f_\mathrm{gc}\left(\mathbf{v}_\mathrm{g},\mathbf{v}_\mathrm{c}\right)$ must be proportional to $\left|\mathbf{v}_\mathrm{g}-\mathbf{v}_\mathrm{c}\right|$. In addition, the distribution function $f_\mathrm{gc}\left(\mathbf{v}_\mathrm{g},\mathbf{v}_\mathrm{c}\right)$ must be proportional to the probability that g and c have the velocities $\mathbf{v}_\mathrm{g}$ and $\mathbf{v}_\mathrm{c}$, respectively, which are the Maxwell-Boltzmann distributions. The total distribution is therefore found to be

$$f_\mathrm{gc}\left(\mathbf{v}_\mathrm{g},\mathbf{v}_\mathrm{c}\right) = \gamma\left|\mathbf{v}_\mathrm{g}-\mathbf{v}_\mathrm{c}\right|\exp\left(-\frac{m_\mathrm{g}\mathbf{v}_\mathrm{g}^2}{2k_\mathrm{B}T_\mathrm{g}}\right)\exp\left(-\frac{m_\mathrm{c}\mathbf{v}_\mathrm{c}^2}{2k_\mathrm{B}T_\mathrm{c}}\right), \tag{46}$$

where the normalization constant is

$$\gamma = \frac{1}{\sqrt{8\pi}}k_\mathrm{B}^{-3/2}\frac{\sqrt{\dfrac{m_\mathrm{g}}{T_\mathrm{g}}+\dfrac{m_\mathrm{c}}{T_\mathrm{c}}}}{\dfrac{T_\mathrm{g}}{m_\mathrm{g}}+\dfrac{T_\mathrm{c}}{m_\mathrm{c}}}. \tag{47}$$

Integrating over all possible velocities, the average energy transfer is

$$\begin{aligned}\left\langle\Delta E\right\rangle_{T_\mathrm{g},T_\mathrm{c}} &= \int_{-\infty}^{\infty}\int_{-\infty}^{\infty}\Delta E f_\mathrm{gc}\left(\mathbf{v}_\mathrm{g},\mathbf{v}_\mathrm{c}\right)\mathrm{d}\mathbf{v}_\mathrm{g}\mathrm{d}\mathbf{v}_\mathrm{c}\\ &= \int_{-\infty}^{\infty}\int_{-\infty}^{\infty}\frac{m_\mathrm{c}}{2}\left(\left(\mathbf{v}_\mathrm{c}+\frac{2\left(\mathbf{v}_\mathrm{g}-\mathbf{v}_\mathrm{c}\right)}{1+m_\mathrm{c}/m_\mathrm{g}}\right)^2-\mathbf{v}_\mathrm{c}^2\right)\\ &\quad\times f_\mathrm{gc}\left(\mathbf{v}_\mathrm{g},\mathbf{v}_\mathrm{c}\right)\mathrm{d}\mathbf{v}_\mathrm{g}\mathrm{d}\mathbf{v}_\mathrm{c}\\ &= 4\frac{m_\mathrm{g}m_\mathrm{c}}{\left(m_\mathrm{g}+m_\mathrm{c}\right)^2}k_\mathrm{B}\left(T_\mathrm{g}-T_\mathrm{c}\right).\end{aligned} \tag{48}$$

(The energy transfer is obtained by insertion of Eq. (45) into Eq. (44).) This is in agreement with the Baule expression [36,37]. The expression is in accord with thermodynamics in the sense that energy is transferred from the warmer to the colder species.

As an alternative derivation of the average energy transfer, instead of considering $\mathbf{v}_\mathrm{g}$ and $\mathbf{v}_\mathrm{c}$ as the independent variables, $\mathbf{v}_\mathrm{c}$ and the relative velocity $\mathbf{v}_\mathrm{R}=\mathbf{v}_\mathrm{g}-\mathbf{v}_\mathrm{c}$ can be used. The change in $\mathbf{v}_\mathrm{c}$ is determined by the relative motion only,

$$\Delta\mathbf{v}_\mathrm{c} = \frac{2\mathbf{v}_\mathrm{R}}{1+m_\mathrm{c}/m_\mathrm{g}}. \tag{49}$$

The probability distribution of $\mathbf{v}_\mathrm{R}$ in a collision is obtained by integration of f_gc over all points $\left(\mathbf{v}_\mathrm{g},\mathbf{v}_\mathrm{c}\right)=\left(\mathbf{v}_\mathrm{g},\mathbf{v}_\mathrm{g}-\mathbf{v}_\mathrm{R}\right)$:

$$\begin{aligned}f_\mathrm{R}\left(\mathbf{v}_\mathrm{R}\right) &= \int_{-\infty}^{\infty}f_\mathrm{gc}\left(\mathbf{v}_\mathrm{g},\mathbf{v}_\mathrm{g}-\mathbf{v}_\mathrm{R}\right)\mathrm{d}\mathbf{v}_\mathrm{g}\\ &= \gamma\int_{-\infty}^{\infty}\left|\mathbf{v}_\mathrm{R}\right|\exp\left(-\frac{m_\mathrm{g}\mathbf{v}_\mathrm{g}^2}{2k_\mathrm{B}T_\mathrm{g}}\right)\exp\left(-\frac{m_\mathrm{c}\left(\mathbf{v}_\mathrm{g}-\mathbf{v}_\mathrm{R}\right)^2}{2k_\mathrm{B}T_\mathrm{c}}\right)\mathrm{d}\mathbf{v}_\mathrm{g}\\ &\propto \left|\mathbf{v}_\mathrm{R}\right|\exp\left(-\frac{\alpha\mathbf{v}_\mathrm{R}^2}{2k_\mathrm{B}}\right)\end{aligned} \tag{50}$$

where

$$\alpha = \frac{\dfrac{m_\mathrm{g}}{T_\mathrm{g}}\dfrac{m_\mathrm{c}}{T_\mathrm{c}}}{\dfrac{m_\mathrm{g}}{T_\mathrm{g}}+\dfrac{m_\mathrm{c}}{T_\mathrm{c}}}. \tag{51}$$

In the case when the temperatures are equal, the parameter α becomes μ/T where μ is the reduced mass of the colliding particles. The energy transfer in a collision is again equation (44) and hence, in contrast to $\Delta\mathbf{v}_\mathrm{c}$, ΔE depends on both $\mathbf{v}_\mathrm{c}$ and $\mathbf{v}_\mathrm{R}$. Consequently, the distribution of $\mathbf{v}_\mathrm{c}$ conditional the relative velocity $\mathbf{v}_\mathrm{R}$ must be known in order to calculate the average energy transfer. This distribution is given by the probability of a collision with the velocities $\mathbf{v}_\mathrm{c}$ and $\mathbf{v}_\mathrm{R}$ divided by all collisions with the relative velocity $\mathbf{v}_\mathrm{R}$:

$$f_{\mathrm{c}|\mathrm{R}}\left(\mathbf{v}_\mathrm{c}|\mathbf{v}_\mathrm{R}\right) = \frac{f_{\mathrm{gc}}\left(\mathbf{v}_\mathrm{c}+\mathbf{v}_\mathrm{R},\mathbf{v}_\mathrm{c}\right)}{\int\limits_{-\infty}^{\infty} f_{\mathrm{gc}}\left(\mathbf{v}_\mathrm{c}+\mathbf{v}_\mathrm{R},\mathbf{v}_\mathrm{c}\right)\mathrm{d}\mathbf{v}_\mathrm{c}}$$
$$= \frac{|\mathbf{v}_\mathrm{R}|\exp\left(-\frac{m_\mathrm{g}(\mathbf{v}_\mathrm{c}+\mathbf{v}_\mathrm{R})^2}{2k_\mathrm{B}T_\mathrm{g}}\right)\exp\left(-\frac{m_\mathrm{c}^2\mathbf{v}_\mathrm{c}^2}{2k_\mathrm{B}T_\mathrm{c}}\right)}{\int\limits_{-\infty}^{\infty}|\mathbf{v}_\mathrm{R}|\exp\left(-\frac{m_\mathrm{g}(\mathbf{v}_\mathrm{c}+\mathbf{v}_\mathrm{R})^2}{2k_\mathrm{B}T_\mathrm{g}}\right)\exp\left(-\frac{m_\mathrm{c}^2\mathbf{v}_\mathrm{c}^2}{2k_\mathrm{B}T_\mathrm{c}}\right)\mathrm{d}\mathbf{v}_\mathrm{c}}$$
$$\propto \exp\left(-\frac{\left(\mathbf{v}_\mathrm{c}+\delta\mathbf{v}_\mathrm{R}\right)^2}{2\lambda^2}\right) \quad (52)$$

where

$$\delta = \frac{\frac{m_\mathrm{g}}{T_\mathrm{g}}}{\frac{m_\mathrm{g}}{T_\mathrm{g}}+\frac{m_\mathrm{c}}{T_\mathrm{c}}} \quad (53)$$

and

$$\lambda = \sqrt{\frac{k_\mathrm{B}}{\frac{m_\mathrm{g}}{T_\mathrm{g}}+\frac{m_\mathrm{c}}{T_\mathrm{c}}}}\,. \quad (54)$$

Finally, by integration over all $\mathbf{v}_\mathrm{c}$ and $\mathbf{v}_\mathrm{R}$, the average energy transfer is obtained as

$$\langle\Delta E\rangle_{T_\mathrm{g},T_\mathrm{c}} = \int\limits_{-\infty}^{\infty}\left[\int\limits_{-\infty}^{\infty}\Delta E f_{\mathrm{c}|\mathrm{R}}\left(\mathbf{v}_\mathrm{c}|\mathbf{v}_\mathrm{R}\right)\mathrm{d}\mathbf{v}_\mathrm{c}\right] f_\mathrm{R}\left(\mathbf{v}_\mathrm{R}\right)\mathrm{d}\mathbf{v}_\mathrm{R}$$
$$= \int\limits_{-\infty}^{\infty}\left[\int\limits_{-\infty}^{\infty}\frac{m_\mathrm{c}}{2}\left(\left(\mathbf{v}_\mathrm{c}+\frac{2\mathbf{v}_\mathrm{R}}{1+m_\mathrm{c}/m_\mathrm{g}}\right)^2-\mathbf{v}_\mathrm{c}^2\right)\right.$$
$$\left.\times\, f_{\mathrm{c}|\mathrm{R}}\left(\mathbf{v}_\mathrm{c}|\mathbf{v}_\mathrm{R}\right)\mathrm{d}\mathbf{v}_\mathrm{c}\right] f_\mathrm{R}\left(\mathbf{v}_\mathrm{R}\right)\mathrm{d}\mathbf{v}_\mathrm{R}$$
$$= 4\frac{m_\mathrm{g}m_\mathrm{c}}{\left(m_\mathrm{g}+m_\mathrm{c}\right)^2}k_\mathrm{B}\left(T_\mathrm{g}-T_\mathrm{c}\right). \quad (55)$$

The same Baule expression for the average energy transfer is of course found as in equation (48).

Is there any advantage in using the latter procedure to calculate the average energy transfer? Yes, when it comes to simulation there is an advantage. When the collisions are not fully elastic, the calculation of the change in velocities (Eqs. (45, 49)), must be replaced by simulation. Using the first procedure, both $\mathbf{v}_\mathrm{g}$ and $\mathbf{v}_\mathrm{c}$ must be known to calculate $\Delta\mathbf{v}_\mathrm{c}$. With the second procedure, only $\mathbf{v}_\mathrm{R}$ need to be specified in order to calculate $\Delta\mathbf{v}_\mathrm{c}$. The initial cluster translation $\mathbf{v}_\mathrm{c}$ need not be specified until the energy transfer is to be calculated. The important difference is that the simulations may be performed with unspecified translational temperatures.

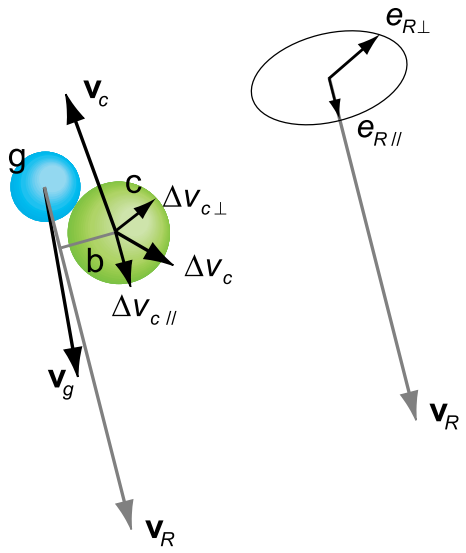

Fig. 14. A collision between the hard spheres g and c is shown. The relative velocity $\mathbf{v}_\mathrm{R} = \mathbf{v}_\mathrm{g} - \mathbf{v}_\mathrm{c}$ is used as a direction of reference. The change of velocity of particle c, $\Delta\mathbf{v}_\mathrm{c}$, is split up in components parallel and perpendicular to $\mathbf{v}_\mathrm{R}$. The unit vectors $\mathbf{e}_{\mathrm{R}_\parallel}$ and $\mathbf{e}_{\mathrm{R}_\perp}$ are defined to be parallel and perpendicular to $\mathbf{v}_\mathrm{R}$. $\mathbf{e}_{\mathrm{R}_\perp}$ is parallel to $\Delta\mathbf{v}_{\mathrm{c}\perp}$.

A.1.2. Collisions in a three-dimensional space

We now turn to the case when the particles g and c move in an infinite three-dimensional space. The derivation of the average energy transfer at the temperatures T_g and T_c follows the procedure with $\mathbf{v}_\mathrm{c}$ and $\mathbf{v}_\mathrm{R}$ as independent variables. In three dimensions, the change in velocity, $\Delta\mathbf{v}_\mathrm{c}$, as well as the energy transfer depend on an extra variable, the impact parameter b. A collision between g (the small particle) and c (the large particle) is illustrated in Figure 14. As a direction of reference we choose the relative velocity $\mathbf{v}_\mathrm{R}$. Let us express the initial velocity of c in one component along $\mathbf{v}_\mathrm{R}$ and one component perpendicular to $\mathbf{v}_\mathrm{R}$

$$\mathbf{v}_\mathrm{c} = \mathbf{v}_{\mathrm{c}_\parallel} + \mathbf{v}_{\mathrm{c}_\perp}. \quad (56)$$

The same is done for the velocity change of c,

$$\Delta\mathbf{v}_\mathrm{c} = \Delta\mathbf{v}_{\mathrm{c}_\parallel} + \Delta\mathbf{v}_{\mathrm{c}_\perp}. \quad (57)$$

Note that $\mathbf{v}_{\mathrm{c}_\perp}$ and $\Delta\mathbf{v}_{\mathrm{c}_\perp}$ are generally not parallel or antiparallel.

At the maximal impact parameter the energy transfer vanishes. This happens when b is the sum of the radii of the hard spheres. The maximal impact parameter is denoted b_max. In a collisions with the impact parameter b

and the relative speed $v_{\mathrm{R}} = |\mathbf{v}_{\mathrm{R}}|$ the change in velocity of particle c may be shown to satisfy

$$\Delta\mathbf{v}_{\mathrm{c}_\parallel} = \frac{2v_{\mathrm{R}}}{1+m_{\mathrm{c}}/m_{\mathrm{g}}}\left(1-\frac{b^2}{b_{\max}^2}\right)\mathbf{e}_{\mathrm{R}_\parallel}, \tag{58}$$

$$\Delta\mathbf{v}_{\mathrm{c}_\perp} = \frac{2v_{\mathrm{R}}}{1+m_{\mathrm{c}}/m_{\mathrm{g}}}\frac{b}{b_{\max}}\sqrt{1-\frac{b^2}{b_{\max}^2}}\mathbf{e}_{\mathrm{R}_\perp}, \tag{59}$$

where $\mathbf{e}_{\mathrm{R}_\parallel}$ and $\mathbf{e}_{\mathrm{R}_\perp}$ are unit vectors parallel and perpendicular to $\mathbf{v}_{\mathrm{R}}$, respectively. The precise direction of $\mathbf{e}_{\mathrm{R}_\perp}$ depends on where g hits c. When $\mathbf{v}_{\mathrm{c}}$ and $\Delta\mathbf{v}_{\mathrm{c}}$ are expressed in its components, the energy transfer is

$$\begin{aligned}\Delta E &= \frac{m_{\mathrm{c}}}{2}\left(\left(\mathbf{v}_{\mathrm{c}_\parallel}+\mathbf{v}_{\mathrm{c}_\perp}+\Delta\mathbf{v}_{\mathrm{c}_\parallel}+\Delta\mathbf{v}_{\mathrm{c}_\perp}\right)^2-\left(\mathbf{v}_{\mathrm{c}_\parallel}+\mathbf{v}_{\mathrm{c}_\perp}\right)^2\right)\\ &= \frac{m_{\mathrm{c}}}{2}\left(\left(\mathbf{v}_{\mathrm{c}_\parallel}+\Delta\mathbf{v}_{\mathrm{c}_\parallel}\right)^2+\left(\mathbf{v}_{\mathrm{c}_\perp}+\Delta\mathbf{v}_{\mathrm{c}_\perp}\right)^2-\mathbf{v}_{\mathrm{c}_\parallel}^2-\mathbf{v}_{\mathrm{c}_\perp}^2\right).\end{aligned} \tag{60}$$

The simplification in the last step in equation (60) is possible since some of the vectors are perpendicular.

Let us now calculate the average energy transfer at fixed $\mathbf{v}_{\mathrm{R}}$ and b. Integration is required over the velocities $\mathbf{v}_{\mathrm{c}_\parallel}$, $\mathbf{v}_{\mathrm{c}_\perp}$ and $\Delta\mathbf{v}_{\mathrm{c}_\perp}$ in equation (60) but there is no need for integration over $\Delta\mathbf{v}_{\mathrm{c}_\parallel}$ since it is fixed at fixed $\mathbf{v}_{\mathrm{R}}$ and b. We have not been able to calculate the conditional probability $f_{\mathrm{c}|\mathrm{R}}(\mathbf{v}_{\mathrm{c}}|\mathbf{v}_{\mathrm{R}})$ analytically, but from a computer experiment where we generated random velocities $\mathbf{v}_{\mathrm{g}}$ and $\mathbf{v}_{\mathrm{c}}$, we were able to determine the distribution when $\mathbf{v}_{\mathrm{c}}$ is expressed in its components:

$$f_{\mathrm{c}_\parallel|\mathrm{R}}\left(\mathbf{v}_{\mathrm{c}_\parallel}|\mathbf{v}_{\mathrm{R}}\right) \propto \exp\left(-\frac{\left(\mathbf{v}_{\mathrm{c}_\parallel}+\delta\mathbf{v}_{\mathrm{R}}\right)^2}{2\lambda^2}\right), \tag{61}$$

$$f_{\mathrm{c}_\perp|\mathrm{R}}\left(\mathbf{v}_{\mathrm{c}_\perp}|\mathbf{v}_{\mathrm{R}}\right) \propto \exp\left(-\frac{\mathbf{v}_{\mathrm{c}_\perp}^2}{2\lambda^2}\right), \tag{62}$$

where δ and λ are the same as in equations (53, 54). The distribution of $\mathbf{v}_{\mathrm{c}_\parallel}$ is equivalent to equation (52) in one dimension. The rotations of $\mathbf{v}_{\mathrm{c}_\perp}$ and $\Delta\mathbf{v}_{\mathrm{c}_\perp}$ around $\mathbf{v}_{\mathrm{R}}$ are uniformly distributed but the norm of $\Delta\mathbf{v}_{\mathrm{c}_\perp}$ is fixed at fixed $\mathbf{v}_{\mathrm{R}}$ and b. The integral of ΔE at fixed $\mathbf{v}_{\mathrm{R}}$ and b turns out to be independent of the direction on $\mathbf{v}_{\mathrm{R}}$, but depends on v_{R}

$$\langle\Delta E\rangle_{b,v_{\mathrm{R}}} = \int \Delta E f\left(\mathbf{v}_{\mathrm{c}_\parallel},\mathbf{v}_{\mathrm{c}_\perp},\Delta\mathbf{v}_{\mathrm{c}_\perp}|v_{\mathrm{R}},b\right)\mathrm{d}\Delta v_{\mathrm{c}_\perp}\mathrm{d}v_{\mathrm{c}_\parallel}\mathrm{d}v_{\mathrm{c}_\perp} \tag{63}$$

$\langle\Delta E\rangle_{b,v_{\mathrm{R}}}$ is obtainable and is given by a long analytical expression.

The next step is to integrate $\langle\Delta E\rangle_{b,v_{\mathrm{R}}}$ over v_{R} in order to obtain the average energy transfer at fixed b. The derivation of the distribution of v_{R} is similar to the one in one dimension (Eq. (50)). The distribution of the relative velocity in the x dimension of all pairs of particles (not only colliding particles) is (compare to Ref. [32])

$$f\left(\mathbf{v}_{\mathrm{R},x}\right) \propto \exp\left(-\frac{\alpha\mathbf{v}_{\mathrm{R},x}^2}{2k_{\mathrm{B}}}\right). \tag{64}$$

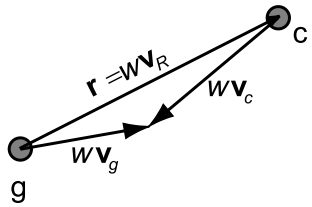

Fig. 15. All particles c along the vector $w\mathbf{v}_{\mathrm{R}}$ will collide with the particle g during the time w.

where α is the same as in the one-dimensional case (Eq. (51)). The motions in the different dimensions are independent which implies that

$$f\left(\mathbf{v}_{\mathrm{R}}\right) \propto \exp\left(-\frac{\alpha\mathbf{v}_{\mathrm{R}}^2}{2k_{\mathrm{B}}}\right). \tag{65}$$

However, in order to obtain the distribution of velocities in collisions, equation (65) has to be modified to account for the fact that collisions between pairs of particles with a high relative speed occur more frequently. In Figure 15, one particle g is at the origin. All particles c that collide with g during the time period w are counted. The particles c must initially be on a straight line from the origin to $\mathbf{r} = w\mathbf{v}_{\mathrm{R}}$ in order to collide. Thus, a factor $|\mathbf{v}_{\mathrm{R}}|$ which is proportional to the number of particles c along $\mathbf{r}$ must be multiplied with the distribution in equation (65) to give the distribution of relative velocity of colliding particles:

$$f\left(\mathbf{v}_{\mathrm{R}}\right) \propto |\mathbf{v}_{\mathrm{R}}| \exp\left(-\frac{\alpha\mathbf{v}_{\mathrm{R}}^2}{2k_{\mathrm{B}}}\right). \tag{66}$$

The distribution of the relative speed is

$$f_R\left(v_{\mathrm{R}}\right) \propto v_{\mathrm{R}}^3 \exp\left(-\frac{\alpha v_{\mathrm{R}}^2}{2k_{\mathrm{B}}}\right). \tag{67}$$

The average energy transfer at fixed b may be obtained as

$$\begin{aligned}\langle\Delta E\rangle_b &= \int_0^\infty \langle\Delta E\rangle_{b,v_{\mathrm{R}}} f_{\mathrm{R}}\left(v_{\mathrm{R}}\right)\mathrm{d}v_{\mathrm{R}}\\ &= 8\left(1-\left(\frac{b}{b_{\max}}\right)^2\right)\frac{m_{\mathrm{g}}m_{\mathrm{c}}}{\left(m_{\mathrm{g}}+m_{\mathrm{c}}\right)^2}k_{\mathrm{B}}\left(T_{\mathrm{g}}-T_{\mathrm{c}}\right).\end{aligned} \tag{68}$$

One can see that $\langle\Delta E\rangle_b$ gradually decreases to zero when b increases to $b_{\max}$. The energy transfer in head-on collisions ($b = 0$ Å), is twice the energy transfer in the one-dimensional space (Eq. (55)). However, integration over all b, where b is distributed according to equation (11) leads to

$$\begin{aligned}\langle\Delta E\rangle_{T_{\mathrm{g}},T_{\mathrm{c}}} &= \int_0^{b_{\max}} \langle\Delta E\rangle_b f_b\left(b\right)\mathrm{d}b\\ &= 4\frac{m_{\mathrm{g}}m_{\mathrm{c}}}{\left(m_{\mathrm{g}}+m_{\mathrm{c}}\right)^2}k_{\mathrm{B}}\left(T_{\mathrm{g}}-T_{\mathrm{c}}\right).\end{aligned} \tag{69}$$

The result is interesting as it is equal to the one-dimensional result. The implication is that in the three-dimensional case, only one dimension is effectively involved in the collisional energy transfer between hard spheres.

A.2. Collisions between Pd_{13} and rare gases

The initial positions and velocities should be randomly generated in order to give the energy transfer at desired gas temperature T_g and cluster temperature T_c. The distribution functions just derived should now be used in order to generate initial translational velocities and impact parameter for the gas-cluster collisions. Two modifications are however employed. First, instead of the true distribution of the impact parameter (Eq. (11)) we have used equation (12). The reason to simulate relatively many trajectories with small b is that these trajectories contribute most significantly to the average energy transfer and the statistical accuracy is thereby enhanced. When calculating the average energy transfer, the use of the "incorrect" $\tilde{f}_b(b)$ will be compensated by an appropriate weight factor.

Second, the initial relative speed should be generated according to equation (67) but instead we have used the normalized function $\tilde{f}_R(v_R)$ which is linear in v_R^2. The distribution $\tilde{f}_R(v_R)$ is a compromise between the distributions in equation (67) in the temperature intervals 100 K $< T_g <$ 900 K and 100 K $< T_c <$ 1 100 K (see Fig. 2). The advantage is that $\tilde{f}_R(v_R)$ can be defined to be independent of the temperatures. An appropriate weight factor $g(b, v_R)$ will make sure that the average energy transfer corresponds to the desired pair of temperatures (T_c, T_g):

$$\langle \Delta E \rangle_{T_g,T_c} = \int_0^\infty \int_0^{b_{max}} \langle \Delta E \rangle_{b,v_R} f_b(b) f_R(v_R) \, db dv_R = \int_0^\infty \int_0^{b_{max}} \langle \Delta E \rangle_{b,v_R} \underbrace{\frac{f_b(b) f_R(v_R)}{\tilde{f}_b(b) \tilde{f}_R(v_R)}}_{g(b,v_R)} \tilde{f}_b(b) \tilde{f}_R(v_R) \, db dv_R. \quad (70)$$

The initial atomic coordinates and velocities relative the center of mass of the cluster must be generated. The probability of a spatial configuration $\mathbf{R} = [x_1, y_1, z_1, x_2, ..., z_{13}]$ is proportional to the Boltzmann factor $\exp(-U(\mathbf{R})/k_B T_c)$. Monte Carlo simulation with fixed temperature has been used to generate initial configurations for the collisions. At a fixed temperature the internal coordinates and the internal velocities are independent of each other. The velocity in the x-direction of an atom in the cluster should be sampled according to [32]

$$f(v_{x,j}) \propto \exp\left(-\frac{m_{Pd} v_{x,j}^2}{2 k_B T_c}\right), \qquad j = 1, ..., 13, \quad (71)$$

with a subsequent subtraction of the center of mass velocity. Analogous sampling applies for the y- and z-directions. The set of internal velocities and the set of spatial configurations are connected to form a set of initial configurations of the cluster.

The following scheme is used to simulate the average energy transfer to the cluster based on N collisions. Particle g refers to the gas atom and c to the cluster.

(i) Generate N spatial configurations of Pd_{13} at fixed T_c using Monte Carlo simulations.

(ii) Generate N sets of internal velocities to the palladium atoms according to equation (71).

(iii) Generate a set of relative velocities $\mathbf{v}_{R,i}$, $i = 1, ..., N$, with the relative speed v_R distributed according to $\tilde{f}_R(v_R)$ in Figure 2.

(iv) Generate b_i according to $\tilde{f}_b(b)$. The gas atom is placed so that the distance to the nearest palladium atom is equal to the cut-off of the LJ potential. The collision is aborted when the rare gas atom again is out of the range of interaction from the cluster.

(v) Run the simulations and calculate $\Delta\mathbf{v}_{c,i}$ for the translational motion of the cluster and $\Delta\mathbf{v}_{g,i}$ which is the change in velocity of the gas atom.

(vi) Set the desired T_g. When the temperatures are chosen, the weight function $g(b_i, v_{R,i}) = f_R(v_{R,i}) f_b(b_i) / \tilde{f}_R(v_{R,i}) \tilde{f}_b(b_i)$ can be calculated for each collision i.

(vii) For each collision, generate the initial $\mathbf{v}_{c_\parallel,i}$ according to $f_{c_\parallel|R}(\mathbf{v}_{c_\parallel}|\mathbf{v}_{R,i})$ in equation (61). Generate $\mathbf{v}_{c_\perp,i}$ with a norm according to $f_{c_\perp|R}(\mathbf{v}_{c_\perp}|\mathbf{v}_R)$ in equation (62) and a random direction of $\mathbf{v}_{c_\perp,i}$.

(viii) Calculate the average energy transfer using the weight $g(b_i, v_{R,i})$

$$\langle \Delta E \rangle_{T_g,T_c} \approx \frac{\sum_i^N \Delta E_i g(b_i, v_{R,i})}{\sum_i^N g(b_i, v_{R,i})}, \quad (72)$$

where the energy transfer to the cluster in collision i is calculated by equation (15–17).

(ix) The average energy transfer for the collisions with $b' < b < b''$ is

$$\langle \Delta E \rangle_{T_g,T_c,b} \approx \frac{\sum_i^{N_b} \Delta E_i g(b_i, v_{R,i})}{\sum_i^{N_b} g(b_i, v_{R,i})} \quad (73)$$

where the sum is over the N_b collisions with $b' < b < b''$.

(x) If desired, restart from (vi).

As seen, the N simulated collisions can be used for different gas temperatures. The temperature of the cluster must however be specified before running the simulations since this temperature is a parameter in the distribution of the initial spatial configuration of the cluster. The simulation scheme is tested in the case of two colliding hard

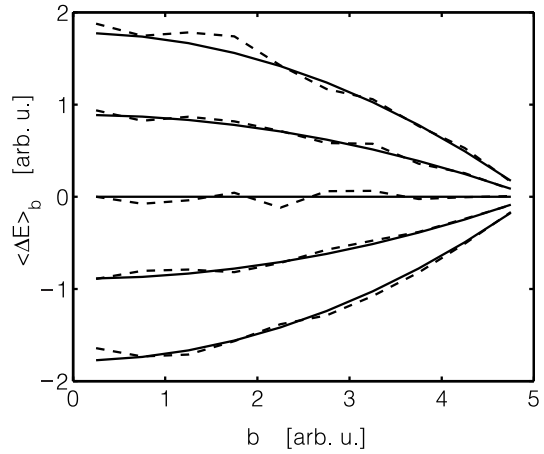

Fig. 16. The average energy transfer in three-dimensional collisions between hard spheres with masses $m_g = 1$ and $m_c = 2$. $k_B T_g = 2$ and from the bottom, $k_B T_c = 1, 1.5, 2, 2.5, 3$. The grey lines show the analytical energy transfer according to equation (65). The black dashed lines show the average energy transfer from 25 000 collisions using the simulation scheme.

spheres in three dimensions with $m_g = 1$, $m_c = 2$ and $k_B T_c = 2$ in dimensionless units. In Figure 16, the average energy transfer to c is drawn *versus* b for a few T_c. The solid curves are obtained according to equation (68) and the dashed curves are obtained by using the simulation scheme with $N = 25\,000$ collisions. Accurate agreement is found.

References

1. M. Homer, J.L. Persson, E.C. Honea, R.L. Whetten, Z. Phys. D **22**, 441 (1991)
2. M. Kappes, M. Schär, U. Röthlisberger, C. Yeretzian, E. Schumacher, Phys. Rev. Lett. **143**, 251 (1988)
3. J. Akola, H. Häkkinen, M. Manninen, Eur. Phys. J. D **9**, 179 (1999)
4. L. Holmgren, M. Andersson, A. Rosén, J. Chem. Phys. **109**, 3232 (1998)
5. W.A. de Heer, P. Milani, A. Châtelain, Phys. Rev. Lett. **65**, 488 (1990); A. Hirt, D. Gerion, I.M.L. Billas, A. Châtelain, W.A. de Heer, Z. Phys. D **40**, 160 (1997)
6. F. Chandezon, P. Hansen, C. Ristori, J. Pedersen, J. Westergaard, S. Bjørnholm, Chem. Phys. Lett. **277**, 450 (1997)
7. M. Schmidt, R. Kusche, W. Kronmüller, B. von Issendorff, H. Haberland, Phys. Rev. Lett. **79**, 99 (1997)
8. J. Westergren, H. Grönbeck, S.-G. Kim, D. Tománek, J. Chem. Phys. **107**, 3071 (1997)
9. J. Westergren, H. Grönbeck, A. Rosén, S. Nordholm, J. Chem. Phys. **109**, 9848 (1998)
10. J. Westergren, H. Grönbeck, A. Rosén, S. Nordholm, Nanostruct. Mat. **12**, 281 (1999)
11. J. Westergren, S. Nordholm, A. Rosén, Phys. Chem. Chem. Phys. (accepted, 2002)
12. R.G. Gilbert, S.C. Smith, *Theory of Unimolecular Reactions* (Blackwell Scientific Publications, Oxford, 1990)
13. S. Nordholm, H.W. Schranz, Adv. Chem. Kin. Dyn. **2a**, 245 (1995)
14. A. Sanches, S. Abbet, U. Heiz, W.-D. Schneider, H. Häkkinen, R.N. Barnett, U. Landmann, J. Phys. Chem. A **103**, 9573 (1999)
15. H. Haberland, Z. Insepov, M. Moseler, Phys. Rev. B **51**, 11061 (1995); H. Haberland, M. Moseler, Y. Qiang, O. Rattunde, Th. Reiners, Y. Thurner, Surf. Rev. Lett. **3**, 887 (1996)
16. H.-P. Cheng, U. Landmann, Science **260**, 1304 (1993)
17. J. Bartels, P. Ten Bruggencate, H. Hausen, K.H. Hellwege, Kl. Schfer, E. Schmidt, *Landolt-Bronstein Zahlenwert und Funktionen* (Springer-Verlag, 1960)
18. H. Haberland, *Clusters of Atoms and Molecules I* (Springer-Verlag, Berlin, 1995), Vol. 52
19. G. Scoles, *Atomic and Molecular Beam Methods* (Oxford University Press, 1992), Vol. 2, p. 231
20. T. Dietz, M. Duncan, D. Powers, R. Smalley, J. Chem. Phys. **74**, 6511 (1981)
21. V. Bondybey, J. English, J. Chem. Phys. **76**, 2165 (1982)
22. J. Jellinek, T.L. Beck, R.S. Berry, J. Chem. Phys. **84**, 2783 (1986)
23. R.S. Berry, T.L. Beck, H.L. Davis, J. Jellinek, Adv. Chem. Phys. **52**, 75 (1988)
24. H.-P. Cheng, X. Li, R.L. Whetten, R.S. Berry, Phys. Rev. A **46**, 791 (1992)
25. W.H. Press, S.A. Teukolsky, W.T. Vetterling, B.P. Flannery, *Numerical Recipies* (Cambridge University Press, Cambridge, 1992)
26. D. Tománek, S. Mukherjee, K.H. Bennemann, Phys. Rev. B **28**, 665 (1983); W. Zhong, Y.S. Li, D. Tománek, Phys. Rev. B **44**, 13053 (1991)
27. A. Münster, *Statistical Thermodynamics* (Springer Verlag, Berlin, 1974), Vol. 2, p. 582
28. A.M. James, M.P. Lord, *Macmillan's Chemical and Physical Data* (Macmillan Press, London, 1992), Table IV.11
29. L.E.B. Börjesson, J. Davidsson, N. Markovic, S. Nordholm, Chem. Phys. **177**, 133 (1993)
30. D.G. Leopold, J. Ho, W.C. Lineberger, J. Chem. Phys. **86**, 1715 (1987)
31. C. Kittel, *Introduction to Solid State Physics* (John Wiley & Sons, New York, 1986)
32. P.W. Atkins, *Physical Chemistry* (Oxford University Press, Oxford, 1986)
33. H. Svedung, N. Markovi, S. Nordholm, Chem. Phys. **248**, 195 (1999)
34. S. Nordholm, L.E.B. Börjesson, L. Ming, H. Svedung, Ber. Bunsenges. Phys. Chem. **101**, 574 (1997)
35. H. Hippler, J. Troe, *Advances in Gas Phase Photochemistry and Kinetics - Bimolecular Collisions*, ed by M.N.R. Ashfold, J.E. Baggott (The Royal Chemical Society, London, 1989), p. 209
36. B. Baule, Ann. Phys. **44**, 145 (1914)
37. T. Brunner, W. Brenig, Surf. Sci. **291**, 192 (1993)